Stony Brook University

Characterization of Anthocyanin Based Dye-Sensitized Organic Solar Cells (DSSC) and Modifications Based on Bio-Inspired Ion Mobility Improvements

A Dissertation Presented

by

Jose Amador Mawyin

to

The Graduate School

in Partial Fulfillment of the

Requirements

for the Degree of

Doctor of Philosophy

in

Materials Science and Engineering

Stony Brook University

May 2009

Stony Brook University

The Graduate School

Jose Amador Mawyin

We, the dissertation committee for the above candidate for the
Doctor of Philosophy degree, hereby recommend
acceptance of this dissertation,

Dr. Charles Fortmann – Dissertation Advisor

Associate Professor – Department of Materials Science and Engineering

Dr. Gary Halada – Chairperson of Defense

Associate Professor – Department of Materials Science and Engineering

Dr. Richard Gambino

Professor – Department of Materials Science and Engineering

Dr. Jon P. Longtin

Associate Professor – Department of Mechanical Engineering

This dissertation is accepted by the Graduate School.

Lawrence Martin
Dean of the Graduate School

Abstract of the Dissertation

Characterization of Anthocyanin Based Dye-Sensitized Organic Solar Cells (DSSC) and Modifications Based on Bio-Inspired Ion Mobility Improvements

by

Jose Amador Mawyin

Doctor of Philosophy

in

Materials Science and Engineering

Stony Brook University

2009

The worldwide electrical energy consumption will increase from currently 10 terawatts to 30 terawatts by 2050. To decrease the current atmospheric CO_2 would require our civilization to develop a 20 terawatts non-greenhouse emitting (renewable) electrical power generation capability. Solar photovoltaic electric power generation is thought to be a major component of proposed renewable energy-based economy.

One approach to less costly, easily manufactured solar cells is the Dye-sensitized solar cells (DSSC) introduced by Greatzel and others. This dissertation describes the work focused on improving the performance of DSSC type solar cells. In particular parameters affecting dye-sensitized solar cells (DSSC) based on anthocyanin pigments extracted from California blackberries (Rubus ursinus) and bio-inspired modifications were analyzed and solar cell designs optimized.

Using off-the-shelf materials DSSC were constructed and tested using a custom made solar spectrum simulator and photoelectric property characterization. This equipment facilitated the taking of automated I-V curve plots and the experimental determination of parameters such as open circuit voltage (V_{OC}), short circuit current (J_{SC}), fill factor(FF), etc. This equipment was used to probe the effect of various modifications such as changes in the annealing time and composition of the of the electrode counter-electrode.

Solar cell optimization schemes included novel schemes such as solar spectrum manipulation to increase the percentage of the solar spectrum capable of generating power in the DSSC. Solar manipulation included light scattering and photon up-conversion. Techniques examined here focused on affordable materials such as silica nanoparticles embedded inside a TiO_2 matrix. Such materials were examined for controlled scattering of visible light and optimize light trapping within the matrix as well as a means to achieve photon up-energy-conversion using the Raman effect in silica nano-particles (due to a strong Raman anti-Stoke scattering probability).

Finally, solutions to the mobility problem of organic photovoltaics were explored. The solutions examined here were based on the bio-inspired neural ionic conduction were nature has overcome the poor ionic mobility in solutions ($D \sim 10^{-5} cm^2/s$) to achieve amazingly fast ionic conduction using non-electric field energy gradients. Electric-permeability-graded layers with possibility to create an energy gradient that helps the diffusion DSSC electrolyte diffusion were explored in this work.

Dedicated to Jose, Marlene, Cristina, Hugo
and those not with us anymore.

Table of Contents

List of Illustrations

List of Equations

List of Tables

Acknowledgements

Graduate school ended up being not precisely what I imagined before joining the program. The glamour of graduate life as seeing from the undergraduate perspective hides the fact that no experiment works right away, the focus of your research can change to more attainable goals and that it doesn't hurt to help with other projects in the lab. I thank these experiences for teaching me about: photonics, phononics, waveguide confinement, shockwaves, nuclear processes, vibration dampening composites, vibrational, X-Ray and electron spectroscopy, ultra high vacuum systems, cicada wings, carbon fiber composites, much cherished teaching experience and photovoltaics.

Many thanks to the people that contributed to this research:

- My advisor Prof. Charles Fortmann for having patience beyond and above the call of duty and because at the end everything comes back to photovoltaics. His interest and breadth of knowledge in this field are a major influence on my current career path. I hope that one day my understanding and contribution to the field of solar energy approaches his level.
- Prof. Gary Halada and Prof. Clive Clayton for taking me aboard their lab and giving me a desk where I could hold court for four years and a half. Their wide-ranging scientific interests broadened my horizons and I thank them for my current interest on sustainable development and bio-inspired materials.
- Prof. Richard Gambino, Prof. Alexander Orlov and Dr. James Quinn for graciously providing access to equipment and facilities that were indispensable for the research presented in this dissertation.
- Prof. Jon Longtin for having the time to be in my committee and offer and external perspective.

I would also like to thank Prof. Harold Metcalf and Dr. John Noe for getting me involved with research and introducing to me the beauty of light. There is a clear path (bumpy and/or meandering) connecting the first time I entered a research lab as an

undergrad to the present. I'm also thankful to Nina, Kathryne and everybody at the Alliance for Graduate Education and the Professoriate (A.G.E.P.) for their support throughout all these years.

Thanks to all the friends I made inside and outside the lab. Their friendship and company was a nice addition to graduate life. Special thanks to all my friends from India, the Caribbean and the rest of the world for their hospitality and for being always welcoming.

Finally, I will like to thank my family and specially my parents and siblings for their support and for always believing that one day I would finish.

1. Introduction

According to a report by the National Renewable Energy Lab (NREL) the worldwide electrical energy consumption will increase from currently 10 terawatts to 30 terawatts by 2050 *[1]*. This projected consumption increase should be placed in contrast with the effects of global warming on humankind. The burning of hydrocarbons that produces a sizeable percentage of the energy in the present also spews greenhouse effect causing gases that will require eons to dissipate. Massive permanent dislocations of human population centers away from the flood prone low-laying areas and the economic resources required are now certain to occur due to the melting of the polar ice and disruption of weather patterns. This will happen even if no more greenhouse gases are added from today going forward. These predicted effects are a powerful driving force in the movement to reduce the levels of greenhouse gases such as CO_2, the number one greenhouse gas in the atmosphere. It is obvious that reducing the current atmospheric CO_2 would require our civilization to develop a 20 terawatts non-greenhouse emitting (renewable) electrical power generation capability. Solar photovoltaic electric power generation is thought to be a major component of proposed renewable energy-based economy.

Solar photovoltaic electric power generation has been known for over sixty years. For the most part photovoltaic solar cells have been fabricated from crystalline silicon and more recently thin film amorphous *[2]* and microcrystalline silicon materials have begun to move into the power generation market place. Silicon-based photovoltaic solar cells have been successful in supplying much of the power for satellite and spacecraft applications and remote power generation such as radio repeaters, roadway signs, and remote housing. However, the high cost of the silicon-based solar cells cost does not compete favorably to traditional CO_2 producing technologies. To achieve the goal of a solar photovoltaic powered future the cost will have to be drastically reduced and manufacturing scales drastically increased.

One approach to less costly, easily manufactured solar cells is the Dye-sensitized solar cells (DSSC) introduced by Greatzel and others *[3-5]*. The DSSC have shown the capacity to compete with silicon-based solar cells on price but poor performance and stability have limited the applications for these cells. However, DSSC's are showing an impressive rate of efficiency improvement compared to other types of photovoltaics being studied or in the market at the present and may soon be high enough to compete with other photovoltaic solar cells and other energy generation methods. This thesis describes the work focused on improving the performance of DSSC type solar cells. In particular parameters affecting dye-sensitized solar cells (DSSC) based on anthocyanin pigments extracted from California blackberries (Rubus ursinus) and bio-inspired modifications were analyzed and solar cell designs optimized.

The starting point for the research presented here was off-the-shelf DSSC construction materials. Analysis required a custom made solar spectrum simulator and an affordable test-bed photoelectric property characterization station. This custom made equipment facilitated the taking of automated I-V curve plots and the determination of parameters such as open circuit voltage (V_{OC}), short circuit current (J_{SC}), fill factor(FF), etc. This equipment was used to probe the effect of various modifications such as changes in the annealing time and composition of the of the electrode counter-electrode.

Solar cell optimization included novel schemes such as solar spectrum manipulation to increase the percentage of the solar spectrum capable of generating power in the DSSC. Solar manipulation included light scattering and photon up-conversion. With an eye towards ultimate energy production costs techniques examined here focused on affordable materials such as silica nanoparticles embedded inside a TiO_2 matrix. Such materials were examined for controlled scattering of visible light and optimize light trapping within the matrix as well as a means to achieve photon up-energy-conversion using the Raman effect in silica nano-particles (due to a strong Raman anti-Stoke scattering probability).

Finally, solutions to the mobility problem of organic photovoltaics were explored. The solutions examined here were based on the bio-inspired -neural ionic conduction (based on previous work by Kang and Fortmann *[6]*) were nature has overcome the poor ionic mobility in solutions ($D \sim 10^{-5} cm^2/s$) to achieve amazingly fast ionic conduction using non-electric field energy gradients. Electric-permeability-graded layers with possibility to create an energy gradient that helps the diffusion DSSC electrolyte diffusion were explored in this work.

2. Photovoltaics

In essence all energy sources, renewable and non-renewable (oil, wind, biomass, solar energy) are directly or indirectly derived from the solar radiation irradiating the planet. The farther downstream the energy is gathered from the initial solar radiation source, the greater the losses due to various conversion inefficiencies. Therefore the most efficient methods harvest energy closest to the sun emitted photons, the original source.

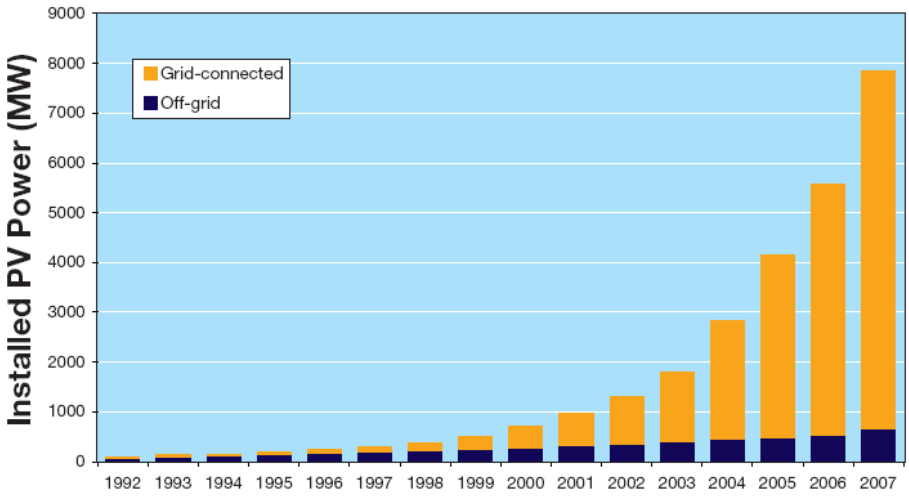

FIGURE 2-1: YEARLY INCREASE OF INSTALLED PHOTOVOLTAIC SYSTEM BY IEA MEMBER COUNTRIES *[7].*

In the United States the number of photovoltaic energy installations has increased by an enormous rate in the last few years as shown in Figure 2-1. For instance, between 2006 to 2007 there was an increase by 42% in photovoltaic systems installation (145 MW to 206.5 MW) *[8]*. This huge increase in the photovoltaics market has sparked the interest of the industry to find opportunities to lower the manufacture cost of solar modules. This will be accomplished by finding technologies such as organic solar cells that are not as energy intensive to neither fabricate nor require expensive, highly purified, and/or scarce materials for their manufacture.

While, solar cells offer an attractive alternative to other renewable energy sources, the mass production of solar cells is an expensive proposition. Typically the cost associated with the amount of land need for solar cells and the cost of support structures decrease with increasing solar cell efficiency. Efficiency is the percentage of solar energy transformed in electrical energy/power by the solar cell. The most expensive photovoltaic system can achieve almost 40% efficiency while the most common mass produced types have an efficiency rating of around 15% (Figure 2-2). The monetary cost of high efficiency solar cells is extremely high. However, if the efficiency is less than ~ 6% the large amounts of land and support structures make their use impractical. Most of the high efficiency solar designs are geared for applications where cost is an issue secondary to power generation such as satellites or equipment in remote unmanned research outpost.

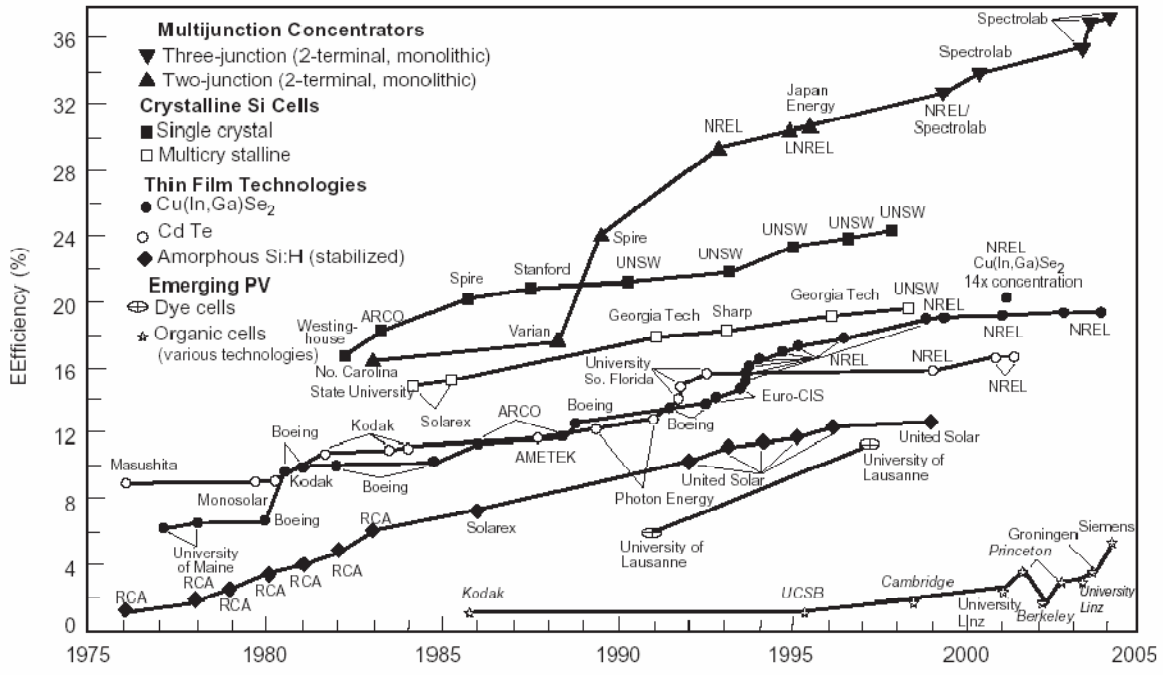

FIGURE 2-2: IMPROVEMENTS IN PHOTOVOLTAIC EFFICIENCY *[9, 10]*

The high cost of these traditional inorganic solar cell designs prohibits their large scale terrestrial energy production; thereby, hindering the goal of a photovoltaic solution

to renewable green energy generation in the United States. DSSC organic solar cells are a promising solution since these do not use the same energy costly materials as inorganic solar cells. It is possible to manufacture them using high throughput techniques similar to rapid printing. Organic cells and dye-sensitized cells, despite their recent introduction are being rapidly optimized. The efficiency has increased to a point where they can compete with other thin-film technologies such as amorphous silicon cells (Figure 2-2).

The work presented in this dissertation is supported by the expertise in photovoltaics research of the Fortmann Research Group that is focused on improving the efficiency of dye-sensitized and thin-film solar cells. The photovoltaics designs currently being researched by the group can be fabricated inexpensively and in great quantities.

3. Physics of Solar Cells

In this section the basics of photovoltaic solar energy conversion are described. In standard (non-DSSC) solar cells a semiconductor absorber is used. Semiconductors optical absorption is dominated by photo induced electronic transitions between two partially occupied electronic bands separated by a band gap in which there are substantially no electronic states. To be useful for absorbing sunlight the band gap must be between ~ 1 and 2 eV, that is, where the largest amount of sunlight energy is available. Photons with less energy than the band gap pass through the semiconductor without absorption possibility.

Incoming photons with energy larger than the band gap create charge carriers by photo-excitation of electron from the valence into the conduction band while leaving a hole behind. The creation of electron-hole pairs results in the loss (absorption) of a photon from the incoming irradiation flux. Beer's law describes the overriding absorption process:

$$\frac{d\Gamma}{dx} \propto -\alpha_\lambda \Gamma$$

or

$$\Gamma_\lambda = \Gamma_{0,\lambda} e^{-\alpha_\lambda x}$$

EQUATION 3-1: BEER'S LAW

Where Γ_λ is the photon flux at a particular wavelength, λ, (or band of wavelengths), α_λ is the absorption constant of the semiconductor at a particular wavelength, and x is the displacement of the photon into the materials. Typically it is desirable to have large absorption coefficients so that the light can be absorbed in a thinner (less expensive) amount of material. Also it is important to recognize that electron-holes pairs generated anywhere with the absorber can lead to a collected (external power generating) charge.

Once a photon creates an electron-hole pair it is necessary to separate the two charge types so that they can be collected at an appropriate contact region and turned into an external electric power. Typical solar cell designs require electrons and holes to either diffuse (a random walk) to their respective contact or in some cases an electric field can be incorporated to help charges "drift" to their respective contacts.

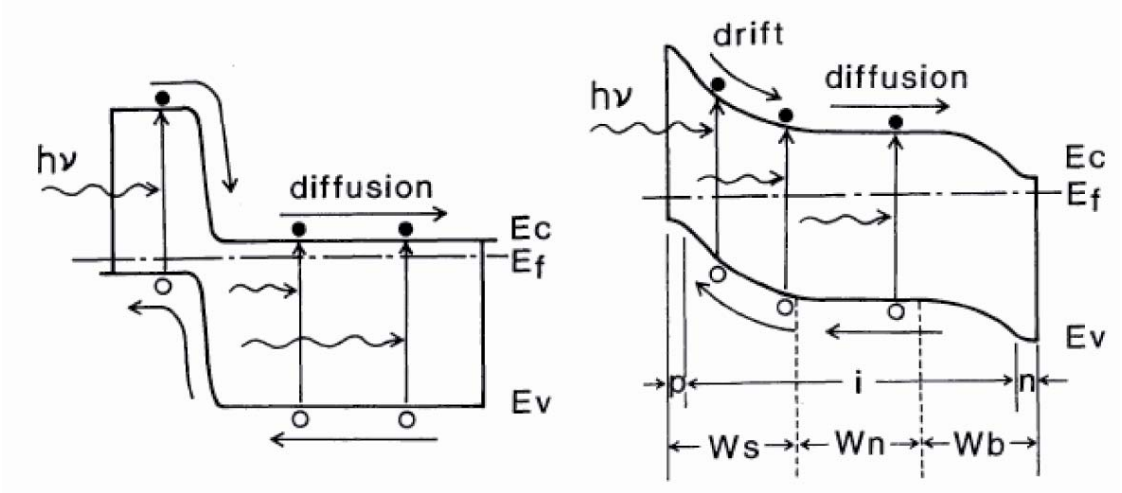

FIGURE 3-1: PHOTO GENERATION AND COLLECTION OF ELECTRON-HOLE PAIRS IN TYPICAL CRYSTALLINE SOLAR CELL (LEFT) AND A TYPICAL AMORPHOUS SILICON SOLAR CELL (RIGHT)

Within the semiconductor regions near the contacts usually consist of heavily doped material, p-type doping for the hole-type contact, and n-type doping for the electron contact. These doped regions serve two purposes: one, to provide regions of high electron and hole probability where each carrier will tend to reside once they arrive there by diffusion and/or drift; and two, a region which due to the high resident carrier concentration easily makes contact to an external metal electrode for power extraction. Electrons and holes may recombine prior to reaching their respective contacts thereby generating an amount of heat (non-radiative recombination) or they may emit a new photon corresponding to all or part of the band-to-band energy with the remaining energy being converted to heat (see e.g.,*[11-13]*). The processes of photo absorption and electron-hole pair collection are shown in Figure 3-1 *[14]*. This figure shows the incorporation of an electric field to help carriers drift to their contacts in the case of a typical amorphous silicon cell (Figure 3-1-Right). The presence of this drift field *[15]* is not necessary in a crystalline silicon cell (Figure 3-1-Left).

Recombined electron-hole pairs do not generate external power and detract from the overall performance of the solar cell. Recombination can always occur within a semiconductor but increases drastically when defects such as impurity atoms, vacancies, and other defects such as surfaces are involved. The best semiconductor solar cells typically employ the most pure crystalline materials.

Materials that exhibit some sort of photovoltaic effect are relatively common. One of the first recorded examples of the photovoltaic effect is the experiment of Becquerel in 1839 who recorded a photovoltage in an electrolyte solution exposed to light *[11]*. The efficiency of these early devices was extremely low and in the range of 1%. Efficiency is defined as the percentage of the incident solar energy that is transformed into electric energy. However, the photovoltaic cell efficiency has been slowly but steadily increasing from the single digits after Becquerel experiment, to around 15% in the 1950's. More recently modern state-of-the-art photovoltaic solar cells can have efficiencies approaching 40% *[11]*.

To produce electric energy from the incoming solar energy a photovoltaic device must be able to generate charge carriers, separate them long enough to avoid recombination and finally must be able to transport them to the output circuitry *[13]*. The carrier production is conceptually simple in the sense that any photon with energy larger than the band gap can excite an electron from the valence into the conduction band. Charge separation is achieved by having layers of semiconductor materials with chemical potential gradients induced by doping. This offset in the energy bands induces an electric field that is the driving force in the separation of generated carriers (electrons and holes).

The photocurrent generated by the solar cell depends on many factors but can be related to:

$$J_{SC} = q\int b_s(E)QE(E)dE$$

EQUATION 3-2: PHOTOCURRENT AS FUNCTION OF INCIDENT LIGHT

where J_{SC} is the photocurrent density, QE is the quantum efficiency and QE(E) is the probability of excitation of an electron by a photon of energy E and $b_s(E)$ is the incident spectral photon flux density *[11]*. Since the absorption coefficient is a function of wavelength the amount of light collected in any particular region of the solar cell is dependent on wavelength. For example, short wavelength light has high energy and tends to have a relatively large absorption coefficient. This high absorption coefficient leads to absorption in the front of the absorber layer near to a surface and/or the highly doped contact region where recombination is high. Consequently, many of the electron-hole pairs generated by short wavelength light are lost due to recombination.

The factors that impact the collection of photo-generated electron-hole pairs can be expressed as an equation relating the diffusion constant, D, electric fields (in any), the absorption constant (as a function of wavelength), the photon flux, and the position within the absorber layer, x. Following Hovel *[16]* the equation for the diffusion case with no drift assisting electric fields in its general solution is:

$$(p_n - p_{n0}) = A\cosh\left(\frac{x}{L_p}\right) + B\sinh\left(\frac{x}{L_p}\right) - \frac{\alpha F(1-R)\tau_p}{(\alpha^2 L_p^2 - 1)}\exp(-\alpha x)$$

EQUATION 3-3: HOVEL'S EQUATION

where $(p_n - p_{n0})$ is the change in excess carrier density, x is the distance from the surface, L_p is the diffusion length, $L_p = (D_p\tau_p)$, α is the absorption constant, τ_p is the hole lifetime, F is the number of incident photons per sec per unit bandwidth and R is the number of photons reflected from the surface *[16]*. Note that since the absorption constant is a function of wavelength the collection is a function of wavelength. In the last ten years or so the solving of equations to predict photo response of solar cells has given way to more advanced techniques involving finite element solutions (e.g., Pennsylvania State University AMPS *[17]*). These computational techniques allow the properties in every region of the absorber region to vary according to its exact composition etc.

A parallel description and equally important level of description for photovoltaic solar cells involves the circuit diagram of Figure 7-1. Here the built in segregation of electrons and holes to their respective contacts can be expressed as a diode, since such segregation necessarily implied unidirectional current flow within the photovoltaic device. Since the various contacts and conduction paths internal and external to the solar cell have a finite resistance a resistor is represented and since charge can flow though the photovoltaic device in the opposite direction (against the built-in fields and or contact biases) albeit with increased resistance a second, "shunt resistor" is also shown.

The circuit model of Figure 7-1 provides the means by which the performances of the solar cell are characterized. This creates a potential difference known as the open-circuit voltage or V_{oc}. The flow of carriers into the external circuit is a current defined as the short circuit current density or J_{sc} *[11]*. This level of description can also be applied to the DSSC that are the basis of this research. The "equivalent circuit" description can be used to model the behavior of a DSSC using idealized parameters such as diode dark current (I_0), diode ideality factor (n), series (R_{Series}) and parallel resistance (R_{Shunt}). These parameters can be used as fitting variables when trying to explain the relationship between the voltage and current produced by the solar cell as the external load is varied from zero (J_{SC}) to infinity (V_{OC}).

The idealized parameters of the "equivalent circuit" model are useful as a predictive tool to explain photovoltaic performance affecting phenomena like charge-carrier recombination at an interface, non-optimum layer thickness, leakage current at the junction and other problems inherent to photovoltaics.

4. Inorganic Photovoltaics (IPV)

Presently, the vast majority of photovoltaic devices are based on inorganic materials with about 95% being based on silicon alone. Alexandre-Edmond Becquerel *[18]* first noticed the photovoltaics effect in 1839 but it was Charles Fritts in 1883 *[19]* that created the first junction. Fritts created the first photovoltaic junction by pressing together thin sheets of selenium and gold. The first modern breakthrough arrived when researchers at Bell Labs found that under room light illumination a "pn" junction diodes produces a photovoltage *[20]*. Photovoltaic research and production has rapidly progressed from the first Bell Lababoratory solar cells with about 6% conversion efficiency to the present day state-of-the-art cells such as that demonstrated by Spectrolab with an efficiency of 40% (as reported by the Department of Energy *[21]*). Figure 4-1 shows the relative absorption efficiency of the solar spectrum for modern photovoltaic systems.

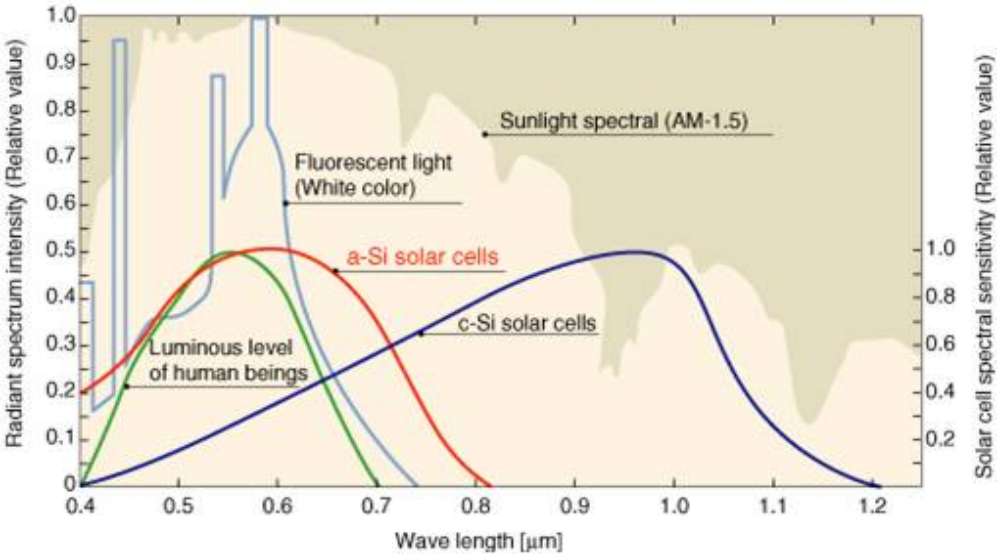

FIGURE 4-1: COMPARISSON BETWEEN SOLAR SPECTRUM AND ABSORPTION RANGE OF IPV

4.1. Single Crystal Solar Cell

Due to a number of historic factors such as the processing technology established to supply the integrated circuits industry and an associated supply of materials (for niche

market applications) silicon has become the present era most dominant solar cell material. Furthermore the low cost of oil over the past two decades has limited the solar cell market to niche applications were high cost is overcome by having no acceptable alternative. The terrestrial solar cell market is based upon single crystal or large grain (> 1 mm) poly-crystalline silicon solar cells *[22]*. In many ways silicon is not the most ideal material has its less than ideal band gap (1.1 eV) and relatively low absorption coefficient leads to the use of thick expensive solar cell absorber layers *[23]*. Nonetheless over the past three decades many techniques have overcome the inherent silicon limitations such as thin-film *[24, 25]* and tandem solar cells *[26, 27]*. Presently silicon-based solar cells are among the highest efficiency solar cells available.

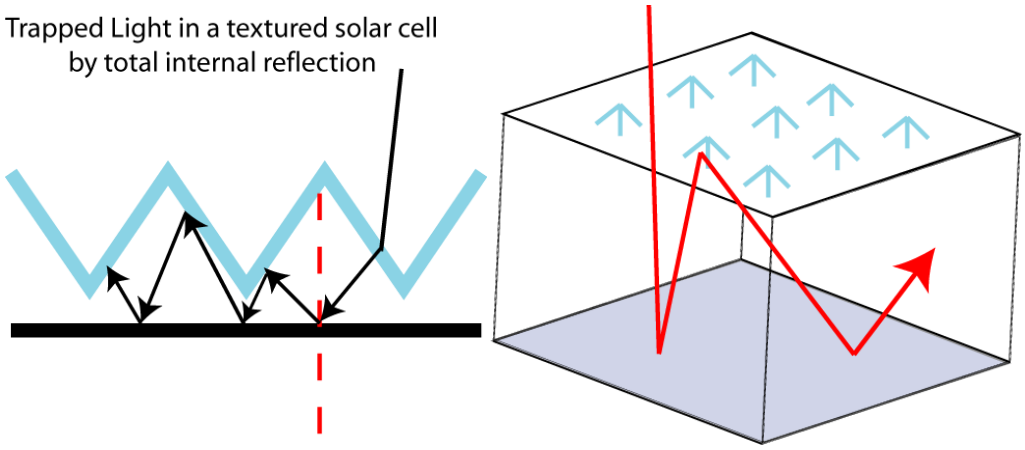

FIGURE 4-2: ILLUSTRATION OF TEXTURED CRYSTALLINE SOLAR CELL.

The current state-of-the-art solar cell has many advanced features for electronic flow optimization and light management within the solar cell. For example, the current state-of-the-art solar cells often employ textured front surfaces to reduce light reflection and thereby increase the amount of light that enters the solar cell for conversion *[28]*. The name "single crystal" refers to the grain size of the material in the device which is presently about 10 cm *[29]*.

High purity, low defect concentration crystalline silicon has low concentrations of recombination centers (recombination centers hinder charge carrier transport as they provide a mechanism through which photo-generated carriers electrons and holes can be lost prior to collection). Almost all aspects of silicon purification, metal contacting schemes, and processing steps are known and automated processing machinery is available *[30]*. Despite the available automation purified silicon is expensive to prepare both monetarily and in energy.

One approach to reducing costs and processing energy needs is to use thinner absorber layers in the solar cell. Naturally, thinner absorber layers would absorber less light that a thicker ones. Reflective layers on the back of the solar cell can reflect un-absorbed light back into the absorber layer *[31]*. Anti-reflection coatings similar to those on camera lens reduce the amount of reflected light and thereby increase the amount of light transmitted into the absorber layer for conversion into electrical power *[32]*. Another solution to reduce the absorber is light trapping surface structure as shown in Figure 4-2 that tend to bend light to large angles that increase the light path length to values much greater than the absorber thickness. These surface structures resemble a pattern of pyramidal structures. Fortunately such structuring of a silicon surface is inexpensive as it can be carried out in a simple chemical etching bath.

The drawback of surface texturing is the increased surface area of the solar cell since the surface is effectively a layer of defects through which photo-generated carriers can be lost due to recombination characterized as an increased effective junction leakage current, $\tilde{J}_0$ defined by $\tilde{J}_0 = junction\ area \times J_0$. Therefore, the effective leakage current increases proportionally with junction area. This recombination lost naturally leads to lower solar cell efficiencies through reduced open circuit voltage (V_{OC}) mentioned before *[33]*. However, it has been demonstrated that although less than ideal surface texturing increases the performance of silicon based solar cells *[34]*.

4.2. Thin film (Polycrystalline) Solar Cells

Single crystals solar cells have shown their potential as photovoltaic devices with high efficiencies and a large share of the photovoltaic market. However, these high efficiencies have a high cost. High costs are not a problem for satellite and remote location applications because of the other extreme costs associated with such endeavors. However, the goal of large-scale terrestrial electric power generation requires competing with oil and coal on a cost basis. Several technologies have emerged as contenders of these low-cost-per-watt applications including the thin-film poly-crystalline solar cell and the amorphous silicon solar cell. Figure 4-3 shows the basic layer stack of a thin-film solar cell.

Materials with lower production cost have been studied including: amorphous silicon (a-Si), microcrystalline thin film silicon (p-Si), polycrystalline thin film cadmium telluride (CdTe), polycrystalline copper indium diselendide (CuInSe2) and others *[35]*. These materials can be easily used to mass produce films by physical or chemical deposition techniques (thin film technologies) *[13]*. However, for a variety of reasons the semi-conducting properties of these films are far inferior to the near perfect transport of highly purified silicon crystal silicon.

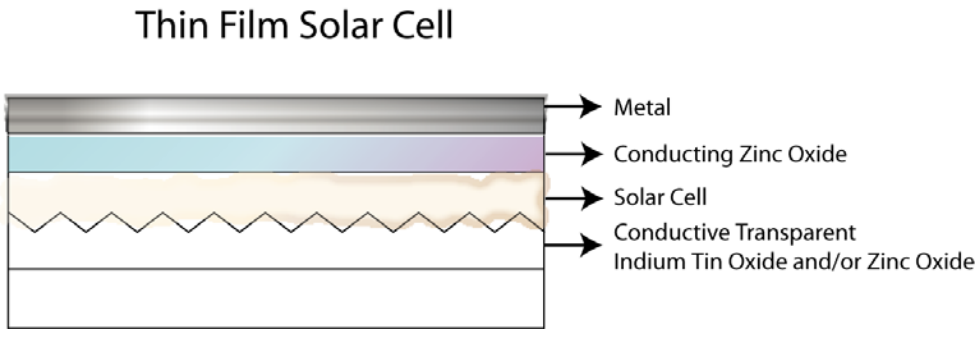

FIGURE 4-3. PROFILE OF THIN FILM SOLAR CELL

The drawbacks of using polycrystalline and amorphous materials are mostly due to the higher concentration of intrinsic defects as compared to crystalline silicon *[36]*. These

defects increase the density of charge carrier traps and recombination centers with effects such as *[13]*:

- Decrease in the diffusion length and lifetime of carriers.
- Higher resistivity due to the increased presence of grain boundaries.
- Presence of defect states in the band gap which can act as carrier traps.

Nonetheless, the thin film absorber used for these types of solar cells (usually less than a few microns and some only a few thousand Angstroms thick) means that photo-generated carriers have less distance to travel and therefore have a relatively low recombination probability *[36, 37]*.

Thin-film compound semiconductor polycrystalline solar cells (Si, CdTe, $CuInSe_2$) have demonstrated significant progress over the last decade with efficiencies reaching almost 20% (Figure 2-2). Drawbacks however remain with questions about the availability of materials, their costs and their toxicity in the CdTe and $CuInSe_2$ cases as well as less (compared to silicon) manufacturing scale-up experience.

Amorphous silicon has emerged as a low cost alternative to single crystal silicon *[38]*. Initially amorphous silicon solar cell research fueled the fundamental research that has lead to a multi-billion dollar industry based on the amorphous silicon-based thin film transistor switched liquid crystal display. Consequently, the industrialization of amorphous silicon solar cell manufacture nearly rival that of single crystal silicon. Importantly while amorphous silicon solar cell efficiencies have reached almost 15% questions about long-term durability persist. Basically all amorphous silicon materials produce photo-generated carrier recombination centers when illuminated under sunlight (Staebler-Wronski effect) *[2, 39]*. Therefore, amorphous solar cells must be made exceeding thin (~ a few thousand Angstroms) in order for the photo-generated carriers to survive long enough to be collected. Since such thin layers do not absorb much light advanced light scattering schemes and multi-junction solar comprised of two or more monolithically stacked amorphous silicon based solar cells have been demonstrated mostly on research solar cells.

5. Organic Photovoltaics (OPV)

Presently organic solar cells are based upon molecules of an organic substance transferring electrons and holes to other materials upon illumination. Therefore, unlike the in-organic solar cells previously described in the organic photovoltaic solar cell individual molecular electron levels are involved in the conversion process rather the spatial continuum of electronic level (electron bands) found in semiconductors *[40]*. Therefore a different understanding needs be applied to the photo generation and charge transport mechanisms found in the organic solar cell. In some cases organic molecules conduct bound photo-generated electron-hole pairs (excitons) as a unit to be reacted and/or separately collected at a location distinct from the point of photo generation.

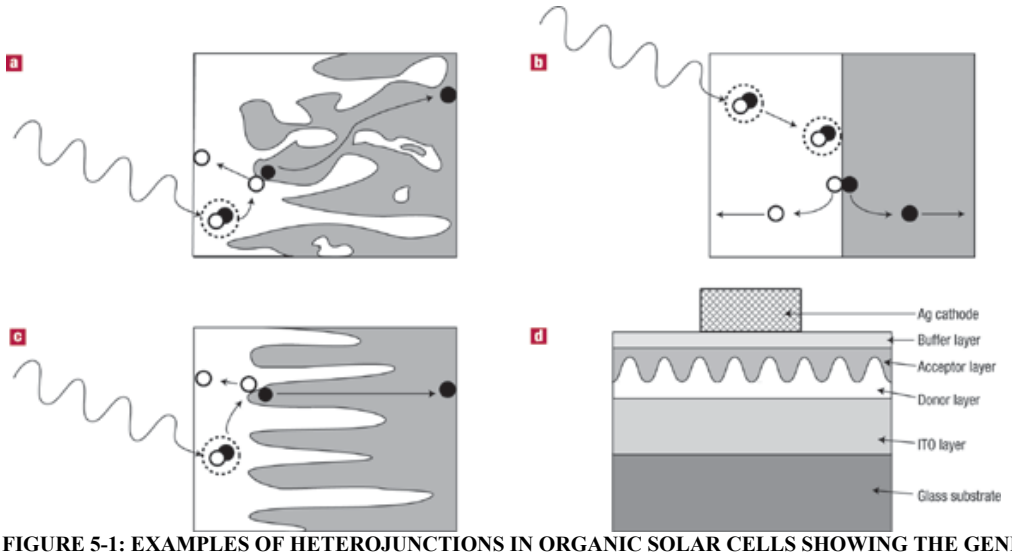

FIGURE 5-1: EXAMPLES OF HETEROJUNCTIONS IN ORGANIC SOLAR CELLS SHOWING THE GENERATION OF EXICTONS IN ONE PHASE AND THE SEPARATION AT AN INTERFACE.

The main difference between organic and inorganic photovoltaics is in how charge carriers are generated. In the case of IPV's both electron and holes are generated throughout the bulk of cell. In the case of OPV's charge carriers are created through a process of photo-generation of excitons and their disassociation into electrons and holes at an interface *[40, 41]*. Organic photovoltaics offer the possibility of a great reduction in the manufacturing cost of the devices compared to IPV's. The manufacturing materials are more readily available (TiO_2, conductive polymers, organic dyes) compared to the quality-control stringent and energy intensive components for IPV's (e.g., silicon single

crystal growth). The nature of the components of OPV's and how they interface together makes them suitable to mass-manufacturing techniques such as screen-printing *[42-44]*and large area spray coatings *[45]*. Depending on their broad characteristics organic photovoltaics depending on their broad characteristics can be divided in the classifications shown in Figure 5-1*[46]*.

5.1. Planar-heterojunction solar cells

Heterojunction solar cells combine conducting polymers (donor and acceptor) with different band gaps. In this case the band gap represents the energy difference between an electron in a binding site and that of the photo generated exciton. The exciton can move through the material in a continuum of levels between neighboring atoms and/or molecules. In this type of OPV the photo-excited charge carriers are bounded in excitons that are not separated until they reach an interface that forms a heterojunction that will separate the electrons and holes chemically and spatially.

The charge separation is due to electrostatic forces arising from electron affinity and ionization potential differences between the two layers. These differences generate a strong electric field that it is enough to separate the bound excitons (~100 meV disassociation energy) if the produce field is strong enough *[47]*. Planar-heterojunctions solar cells as shown in Figure 5-1.b have only a flat interface between the two polymers where the disassociation of the excitons is possible *[48-50]*. This flat interface is a limiting factor in the efficiency of this type of devices.

The efficiency of this type of cell is low (around 1%) compared to the much more efficient semiconductor, bulk-heterojunction, and dye-sensitized solar cells *[51]*. The low efficiency is due to poor exciton transport properties. The diffusion length of the photo-generated excitons (L_D ~50 Å) is smaller than the optical absorption length (~500 Å) by an order of magnitude *[49]*. Therefore, optimization of planar-heterojunction cells is predicated upon a compromise between thick layers to maximize light-absorption for

generation of carriers and thin layers to maximize the number of excitons that reach the interface and are separated.

An alternative is to fold or corrugate the interface as to increase the surface are and reduce the distance travelled by the excitons. Where the amounts of material exposed to the incident light in increased by depositing the photo active material on a microscopically rough surface. This approach can increase the absorption of very thin layers by orders of magnitude. This approach is the inspiration for the next type of organic solar cells.

5.2. Bulk-heterojunction solar cell

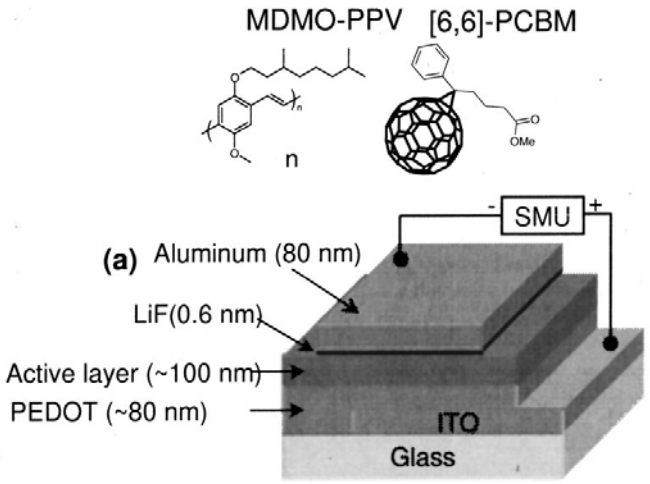

FIGURE 5-2: EXAMPLE OF OPTICAL STACK IN A BULK-HETEROJUNCTION SOLAR CELL *[52].*

Bulk-heterojunction solar cells use an improved interface at the junction to aid in the disassociation of photo-generated excitons as shown in Figure 5-1.a and c. One approach (Figure 5-1.a) involves blending the donor-acceptor materials to form a "disordered" bulk-heterojuncion. The domain size in this blend should be smaller than the diffusion length of the excitons and enough domains should be in contact to form a continuous path to the back-contacts for the transport of the separated charges. Due to the random nature of the interface between the two material the separated charges may end

up in a dead ends where they may be trapped until they recombine with the opposite charge prior to collection *[51]*.

A second approach (Figure 5-1.c) controls more carefully the intermixing between layers by having an interface that fold within itself to create a series of interdigitated fingers. This approach also seeks to decrease the distance that the generated excitons have to travel before reaching the interface. However, this second approach assures a continuous path for the separated charges to the back-contact as compared to the "disordered" type. The extension of the interface into the films increases the opportunity for charge separation *[52-55]*.

In Figure 5-2 it is shown the various layers that compose a bulk-heterojunction cell. The active layer is where the excitons are photo-generated and dissacosiated into electrons and holes. The PEDOT (poly[3,4-(ethylenedioxy)thiophene]) layer is used as a barrier layer (electrons) and hole-only transport layer. These two layers are sandwiched between optimized electron (LiF/Al) and hole (ITO) accepting back contacts *[56]*. The dimensions shown for the layers attest to the need of minimizing the distance that the excitons need to travel before being separated.

5.3. Dye Sensitized Solar Cells

Dye sensitized solar cells (DSSC) as in the case of bulk-heterojunction cells seek to maximize the interfacial area between the donor-acceptor layers by using joined (sintered) nano-particles rather than using the aforementioned convoluting interface. The use of nano-particles also increases the number of photo-generated charge carriers since the donor material (dye) is not used as a bulk layer but instead is a molecular monolayer coating on the surface of an acceptor (TiO_2 in most cases). This leads to an increase in the number of photo-generated carriers as the interfacial layer is up to a thousand times higher in a porous nano-particle film compared to a bulk substrate *[57]*.

DSSC can be seen as an improvement upon photo-electrochemical solar cells (PSC). They are similar in that they contain a photoelectrode, a redox electrolyte and a counter electrode. However, PSC were highly susceptible to degradation of the electrode (Si, GaAs, InP, etc) by the electrolyte *[58]*. DSSC instead use more corrosion resistance oxide semiconductor materials (TiO_2, ZnO and SnO_2) that are sensitized by a dye that generates photo-generated charge carriers that are subsequently separated by electron injection at the dye-oxide interface.

The basic design of DSSC was introduced by Gratzel, O'Regan and others in 1991*[4]*. This design consist of a layer of a semiconductor oxide as an electrode that is sensitized by an organic dye, a layer of a hole-conducting electrolyte, and a layer of a catalytic material that will recycle the oxidized electrolyte as an counter-electrode. Rapid advancements have been made with some of the latest devices reaching an efficiency of 7-10% under AM 1.5 illumination *[59]*.

6. Principles of Dye-Sensitized Solar Cells

A detailed understanding has guided over forty years of semiconductor based photovoltaic where as progress in the DSSC type cell has been carried out under important but as yet in complete descriptions of fundamental processes. This section will review the most significant of these descriptions and processes.

6.1. Internal Processes

The processes inside DSSC that govern the photo-generation and transfer of charges through the different components of the cell can be seen in Figure 6-1. Light enters through the front plate of the DSSC and is absorbed by a molecular monolayer thick dye coating. The dye coating is deposited onto a substrate consisting of sintered TiO_2 nano-particles on a conducting oxide coated glass substrate.

As in the case of the previously described in-organic solar cells when a photon of sufficient energy to excite an electron to an available empty state is incident upon the dye the transition to the upper energy state will occur with a characteristic probability. The photo-generated electrons occupying the upper energy state in the dye are subsequently injected into the conduction band of the oxide (TiO_2) nano-particles on the substrate surface.

Electrons hop through the sintered TiO_2 particle coating until they are injected into the conductive-oxide (TCO) back contact (which has a slightly lower energy level than that of the transporting electron). In-turn the conducting oxide layer is electrically connected to the external load. The electron leave behind a hole that migrates to the counter electrode via a completely independent path involve a liquid sensitizer.

Typically the sensitizer is liquid iodine solution that can absorb a hole by creating a tri-iodine radical.

In effect the sensitizer is oxidized by the photoemission of an electron but its reduced back by electron donation from an iodide molecule (I^-). The iodide oxidizes into a triiodide (I_3^-) but its reduced back to iodide once it diffuses towards the counter-electrode and absorbs an electron coming back through the counter-electrode *[57]*.

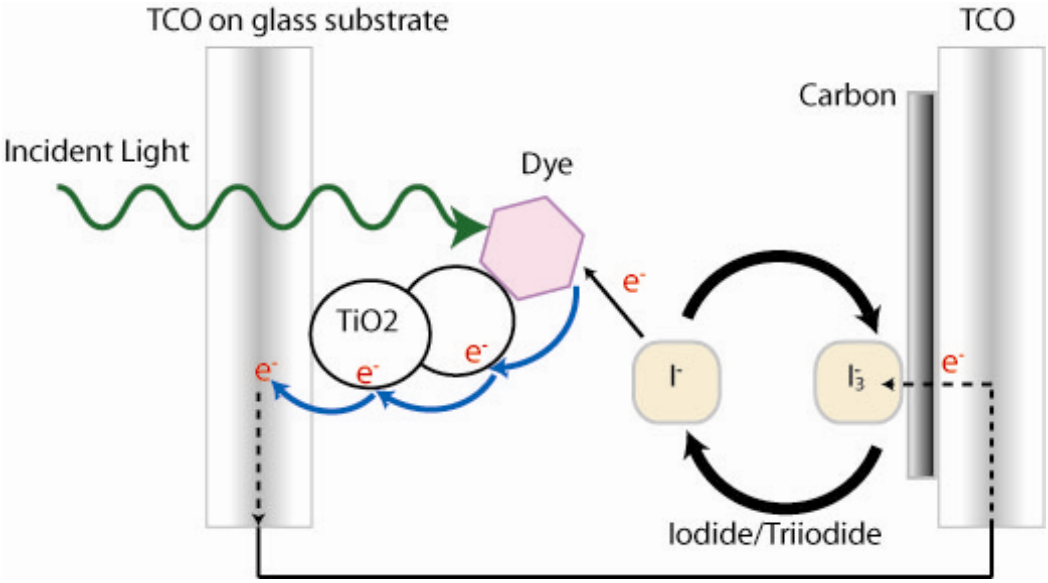

FIGURE 6-1. COMPONENTS OF DSSC AND CURRENT PATHWAY

The following reactions summarize the processes shown in Figure 6-1*[60]*:

1) $dye + light \rightarrow dye^*$ — Absorption of light and photo-excitation of dye

2) $dye^* + TiO2 \rightarrow e^- (TiO_2) +$ oxidized dye — Injection of electron into the oxide and oxidization of dye

3) oxidized dye $+ {}^3/_2\, I^- \rightarrow dye + {}^1/_2\, I_3^-$ — Reduction of dye by electrolyte

4) $^{1}/_{2}\ I_3^- + e^-$ (counter electrode) → $^{3}/_{2}\ I^-$ Reduction of the electrolyte at the counter-electrode

6.2. Potential differences inside dye-sensitized solar cells

There has to be an optimum match between the relative energy levels of the different elements that comprise the DSSC for maximum efficiency. As it is shown in Figure 6-2 the difference between the relative locations of the energy levels create a driving force for the transport of charges. The values shown in Figure 6-2 are electro-chemical potential differences with respect to a reference (Normal Hydrogen Electrode NHE) that is considered to be zero.

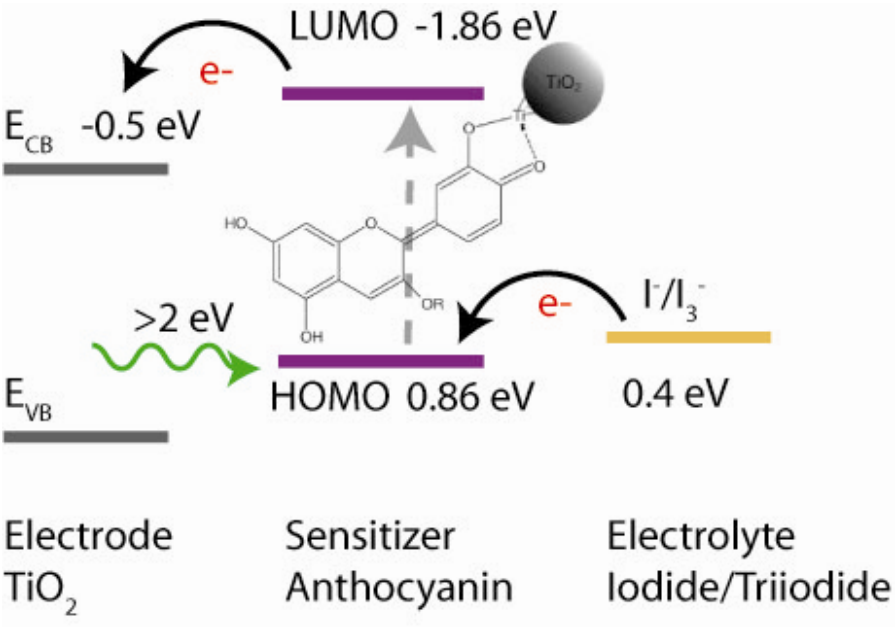

FIGURE 6-2. SCHEMATIC OF ENERGY LEVELS IN COMPONENTS OF DSSC'S. POTENTIALS CALCULATED WITH RESPECT TO A NORMAL OR STANDARD HYDROGEN ELECTRODE (NHE) *[61]*.

The relationship between the potentials of the electrode, sensitizer, counter-electrode and electrolyte is shown in Figure 6-2. These relationships can be summarized as:

- Charge transfer between the electrode and dye corresponds to the photoelectron occupied molecular orbital (HOMO) of the dye decaying to a level within the band-gap of the TiO_2 electrode. In particular excitation decay from the HOMO of the dye to the conduction band of the TiO_2 appear to be the most favorable (i.e., the shortest decay lifetime). Decay of dye photoelectrons to the valance band of the TiO_2 oxide *[41]* while possible do not appear to be probable.

- Optimum charge transfer between the dye and the TiO_2 oxide needs the lowest unoccupied molecular orbital (LUMO) to be located above and near the conduction band of the electrode *[41]*. Charges promoted to this level (LUMO) will be energetically favored to transfer to the conduction band by injection.

- The hole left behind by the is filled by an electron supplied by an iodine ion reaction where electronic charge is injected into the dye forming a charge tri-iodine complex; that is: $3I^- + 2h_{dye} \rightarrow (3I)^- + dye^0$.

- The potential level of the counter-electrode should be close to the equilibrium potential of the redox couple to facilitate the recycling of triiodide, $(3I)^-$ back to iodide (I^-). However, the potential level of the electrode (TiO2) should be higher than the equilibrium potential electrolyte so as to reduce recombination of photoelectrons injected into the TiO_2 oxide with the electrolyte (analogous to a recombination current in a semiconductor solar cell) *[62]*.

6.3. Photovoltage and photocurrent

The origin of the photovoltage in DSSC is not fully understood at the moment. However, as seen on Figure 6-2 it appears to be related to the difference between the conduction band energy level of the oxide (TiO_2) and the redox potential level of the electrolyte *[63, 64]*. The maximum photovoltage that can be theoretically calculated by

considering the various energy levels combined with reasonable estimates internal losses. These losses can be attributed to:

- The dye molecule may lose a proton (and/or hole) by transfer to the oxide (electrode) surface where it will recombine with an injected electron prior to collection *[65]*.

- Other voltage reductions arise from the relative mismatch between the energy levels of the TCO used as a back contact and the electrode, between the HOMO of the dye and the redox couple and finally between the redox couple and the counter-electrode. On the other hand, these differences as shown in Figure 6-2 can aid in the required charge transferes between the various layers of the devices. The losses can also be minimized by a careful selection of the materials with regard to the energy levels.

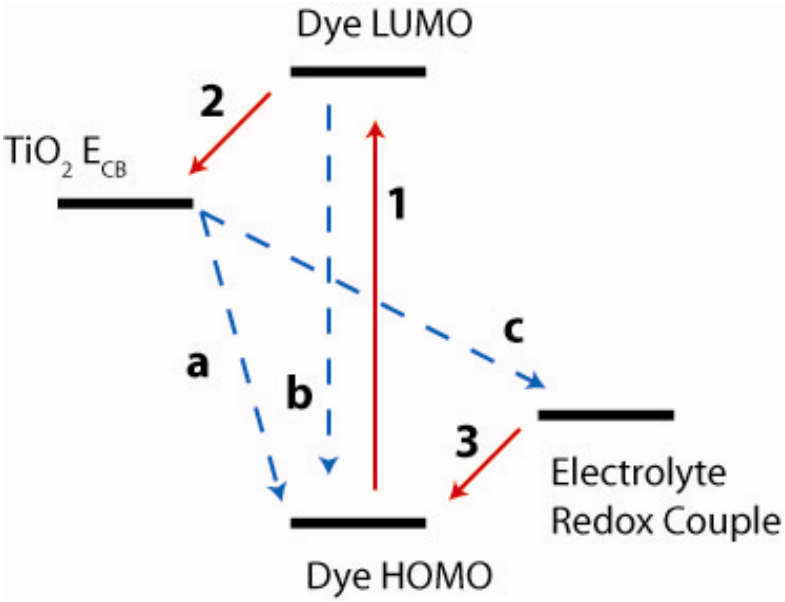

FIGURE 6-3: ELECTRON TRANSFER DYNAMICS INSIDE DSSC. LOSSES SHOWN BY BLUE BROKEN LINES *[66]*

The photocurrent generated is related to the charge injection rate of photo-excited electrons from the HOMO level in the dye to the conduction band minimum (CBM) of the electrode *[41]*. Ideally the electrons inside the DSSC only follow the photo-generation, injection and reduction of the dye cycle (paths 1, 2 and 3 respectively) as

illustrated in Figure 6-3. However, a reduction in the photocurrent by recombination may be caused by the following reasons *[67]*:

- The photo-excited electrons may not be injected into the TiO_2 layer but may remain in the excited state of the dye (LUMO). At this point the electron may decay to the ground state of the dye (Figure 6-3 b); an energy loss mechanism as this transition only produces heat. This probability of this event is low in the DSSC due to the rapid electron injection rate into the TiO_2 layer (femtoseconds) compared to the recombination rate with the electrolyte (microseconds);

- Electrons injected into the TiO_2 layer may recombine with the electrolyte before being collected at the back contact by the reaction $2e^- + I_3^- \rightarrow 3I^-$(Figure 6-3 c) *[68]*. Under short circuit conditions this reaction is too slow to decrease significantly the photo-current. However, under open circuit conditions it serves as the major loss mechanism for photo-generated carriers *[69]*. Increasing the surface area of the TiO_2 particles being covered by the absorbed dye molecules helps to shield the injected electrons form the electrolyte and increases the light absorption within the dye.

7. Equivalent Circuit

As in the case of a typical "np" junction inorganic solar cell it is possible to represent a DSSC with an equivalent circuit model *[66]*. In Figure 7-1 the gray shaded area encloses the components inside a DSSC and U_{int}, U_{ext}, I_{int} and I_{ext} represent the internal voltage, external voltage, internal current and external current respectively. R_{Series}, R_{Shunt} and R_{ext} represent the series resistance from the TCO layers, the shunt resistance of the internal leakage and the external load resistance outside the cell respectively.

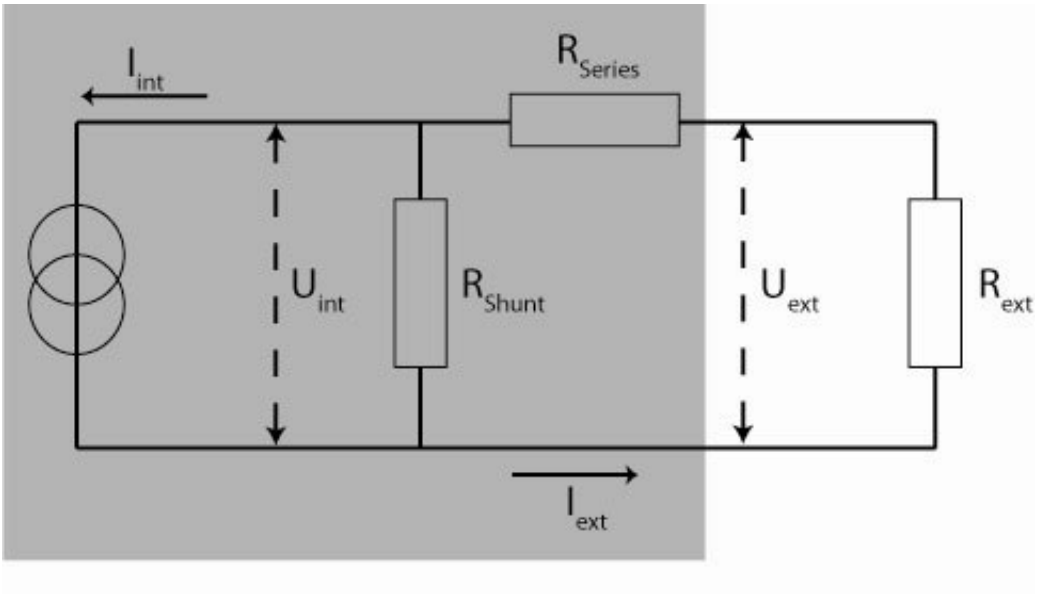

FIGURE 7-1: EQUIVALENT CIRCUIT OF A DSSC

An expression (Equation 7-2) can be derived using the shown equivalent circuit to calculate theoretical I-V curves as a function of parameters from the components shown the equivalent circuit *[70]*.

$$I = I_{ph} - I_d - I_r$$

EQUATION 7-1: COMPONENTS OF THE PHOTOCURRENT

where I_{ph} is the current generated under illumination (approximated to the short circuit current J_{SC}), I_d is the diode current and I_r are the resistance losses. This equation can also be expressed as:

$$I = I_{ph} - I_0 \left\{ e^{q\frac{V+IR_{Series}}{nKT}} - 1 \right\} - \frac{V + IR_{Series}}{R_{Shunt}}$$

EQUATION 7-2: PHOTOCURRENT AND PHOTOVOLTAGE RELATIONSHIP

where I_0 is the saturation current density, R_{Series} and R_{Shunt} are the series and shunt/parallel resistance respectively and n is the diode ideality factor. This equation models the behavior of a solar cell in terms of a diode in the dark but with the current shifted by the photocurrent I_{ph} (Equivalence theorem). That is, the model assumes that the same transport and energy considerations are in effect in the dark and under illumination.

The external current "I" is on both sides of the equation so in order to solve this transcendental function an approximation using the Lambert W-function can be used to solve it numerically. However, an approximation can be made if we consider the R_{Series} term to be small. A series of curves can be plotted to show the effects on the I-V curve of parameters such as series resistance, shunt resistance and the diode factor.

The I-V relation equation has been solved with demonstration values to show how different variables affect the I-V relationship. This can used as an aid interpretation of experimental I-V plots. The following I-V curves where solved using the "Maple 10" (Maplesoft [r]). The transcendental I (I,V) function was solved numerically using the LambertW function built into the software. In the next examples the following test values were used:

R_{Series} = 0.00001 Ohms

R_{Shunt} = 10000 Ohms

I_{ph} = 0.1 Amps

I_0 = 0.000001 Amps

n = 2

k*T/q = 0.0259

7.1. Effect of Series Resistance

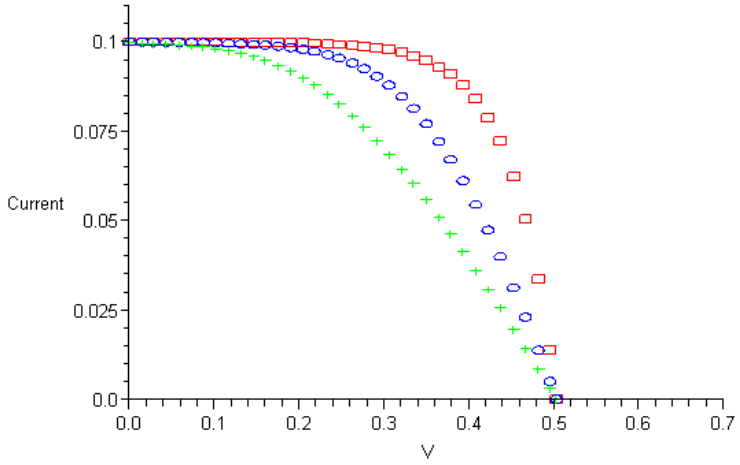

FIGURE 7-2: THEORETICAL I-V CURVE SHOWING EFFECTS OF SERIES RESISTANCE. R_{SERIES} = 0.00001 (SQUARE), 1 (CIRCLE) AND 2 OHMS (CROSS)

There are many contributors to the series resistance but mostly they arise from the charge collection architecture at the front and back surfaces and from the individual layers that make the device (TiO_2, carbon, electrolyte, etc.) and ionic transport across the electrolyte. For example, in DSSC the main source of series resistance is the TCO back-contact layers on the substrate. An increase in the series resistance can be seen as a flattening of the I-V curve and that leads to a decrease in the fill factor and the efficiency (Figure 7-2).

7.2. Effect of Shunt Resistance

Typically, series resistance arise from the materials parameters that make up the solar cell while shunt resistance arise from manufacturing defects. Shunt resistance provide a parallel path for the flow of current (shorting out the cell). In the DSSC they arise from recombination of charges on the surface of the back-contacts and to a lesser amount with charges in the TiO_2 layer with the electrolyte. Care must be taken to reduce these possible paths for recombination. As seen in Figure 7-3 a low shunt resistance flattens the I-V curve and reduces the V_{OC} leading to decreased conversion efficiency.

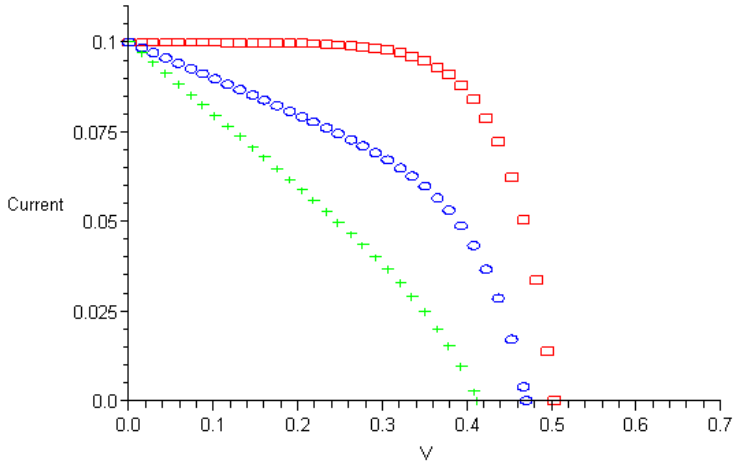

FIGURE 7-3: THEORETICAL I-V CURVE SHOWING EFFECTS OF SHUNT RESISTANCE. RSHUNT = 10000 (SQUARE), 10 (CIRCLE) AND 5 OHMS (CROSS)

7.3. Effect of Diode Factor

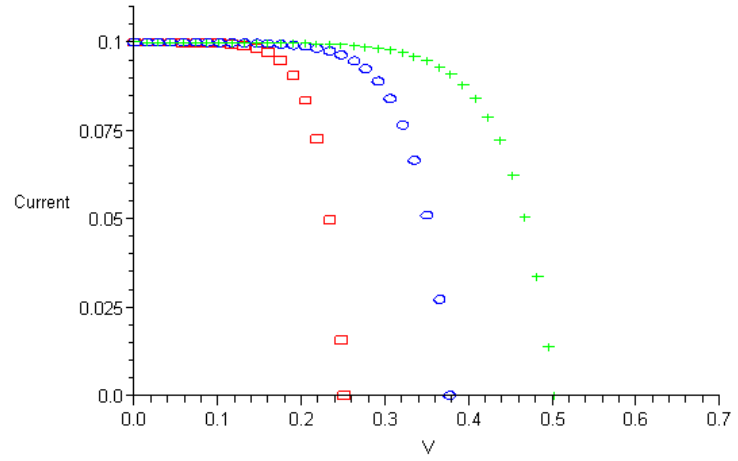

FIGURE 7-4: THEORETICAL I-V CURVE SHOWING EFFECTS OF DIODE FACTOR. N = 1 (SQUARE), 1.5 (CIRCLE) AND 2 (CROSS)

The diode ideality factor, *A*, is a fitting parameter that describes how closely the I-V curve follows a theoretical model. DSSC diode factors range from 1 (close to the ideal case) to 2 depending on the type of carrier recombination present in the cell. As seen in Figure 7-4 a diode factor greater than unity on the I-V curve suggests higher V_{OC} 's implying a greater efficiency. However, this may not be the case since the diode factor is

coupled to other parameters in the cell and in reality it may decrease the performance of the cell through a corresponding decrease in fill factor.

7.4. Effect of Saturation Current

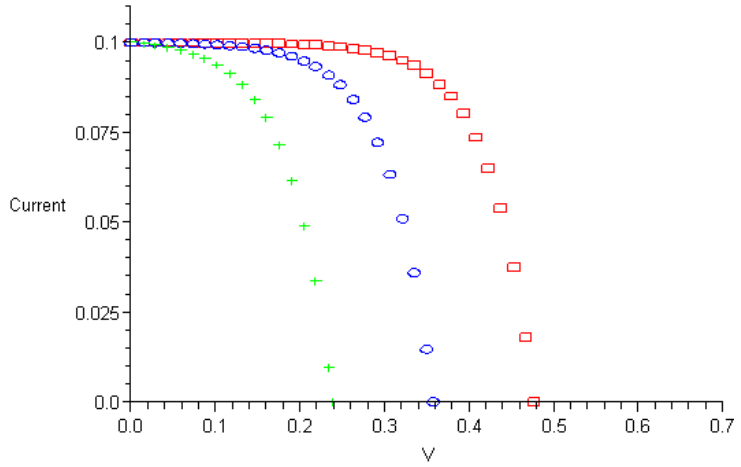

FIGURE 7-5: I-V CURVE SHOWING EFFECTS OF SATURATION CURRENT. I_0 = 0.00001 (SQUARE), 0.0001 (CIRCLE) AND 0.001 AMPS (CROSS)

The saturation current or dark current are parasitic losses related to the ability of the solar cell to maintain charge separation and therefore inhibit recombination losses as a function of voltage. One of the major contributors to these losses occurs at pinholes in the TiO_2 that result in interfaces between the back conducting oxide coating and the electrolyte.

The dark current is related to the shunt resistance as both are a measure of recombination losses within the cell. As it can be seen in Figure 7-5 its effect on the I-V curve is similar to changes in the diode factor. An increase in the saturation current reduced the V_{OC} which leads to a reduction in the cell efficiency. This is because under an ideal scenario the V_{OC} marks the point where the rate of injected carriers is equal to the rate of recombination within the solar cell. If we add another source of recombination (at the TCO interface), the equilibrium between sources (photogeneration) and sink (recombination) of carriers will occur at a reduced bias voltage. The relation between the

open circuit voltage and the saturation current can be expressed as shown in Equation 7-3 *[71]*.

$$V_{OC} = \frac{kT}{q} \ln \frac{I_{SC}}{I_0}$$

EQUATION 7-3: RELATION BETWEEN OPEN CIRCUIT VOLTAGE AND SATURATION CURRENT.

7.5. Characterization Parameters of Solar Cells

The parameters that govern DSSC can be understood better by considering the molecular level rather than the equivalent circuit level. At the molecular level of understanding the output voltage and current are based on the density and mobility of carriers, electrolyte diffusion, absorption cross-section of the absorbed dye, etc *[72]*. This approach proved difficult in this study because some of these parameters were not known and not present in the available literature. In this section where possible molecular level descriptions will be interwoven with equivalent circuit parameters to gain greater insight into the mechanisms and paths for optimization of solar cell performance.

7.5.1. Shunt Resistance

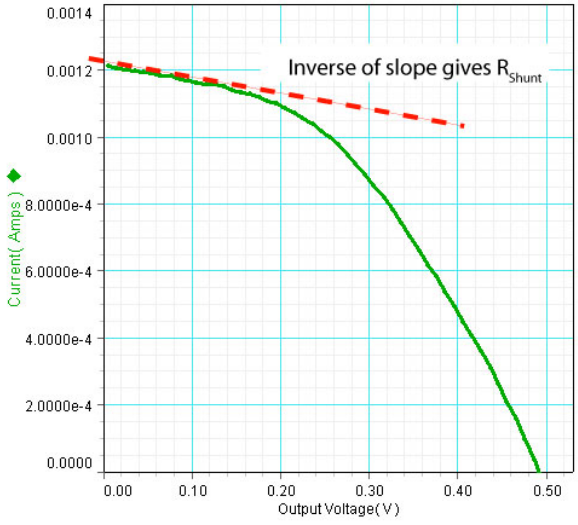

FIGURE 7-6: GRAPHICAL METHOD TO DETERMINE SHUNT RESISTANCE

The shunt resistance can easily be determined using a graphical approach *[73, 74]*. It is the inverse of the slope of the I-V curve on the low voltage region situated at the point of the short circuit current ($I=I_{SC}$, $V=0$) as seen in Figure 7-6.

7.5.2. Series Resistance

Different methods have been proposed to estimate the value of R_{Series}. One method involves taking measurements at different illumination levels and measure the change in the slope between the different curves assuming that the photovoltage drop (V_{OC}) is illumination dependent *[75, 76]*. The method that we have chosen relies on the information from a single curve at normal illumination. This technique is simple and let us experimental quantify R_{Series} from the data gathered in the I-V trace of the cells at normal illumination. The approximation that we are using is a derivation of Equation 7-4 that is valid when I_0 is much smaller than I_{SC} *[77]*. Most of the parameters needed to solve Equation 7-4 can be found experimentally. However, there are no simple analytical solutions for the diode factor "n" and the literature quotes values ranging between 1 and 3 *[70, 74]*. Therefore, the values of DSSC R_{Series} were calculated for n equal to 1 or 3 as to bracket the range of possible values.

$$R_{Series} = \frac{V_{\max}}{I_{\max}} - \frac{nkT}{q(I_{SC} - I_{\max})}$$

EQUATION 7-4: APPROXIMATION USED TO FIND RSERIES

7.5.3. Fill Factor

$$FF = \frac{P_{\max}}{J_{SC}V_{OC}} = \frac{I_{\max}V_{\max}}{J_{SC}V_{OC}}$$

EQUATION 7-5: FILL FACTOR EQUATION

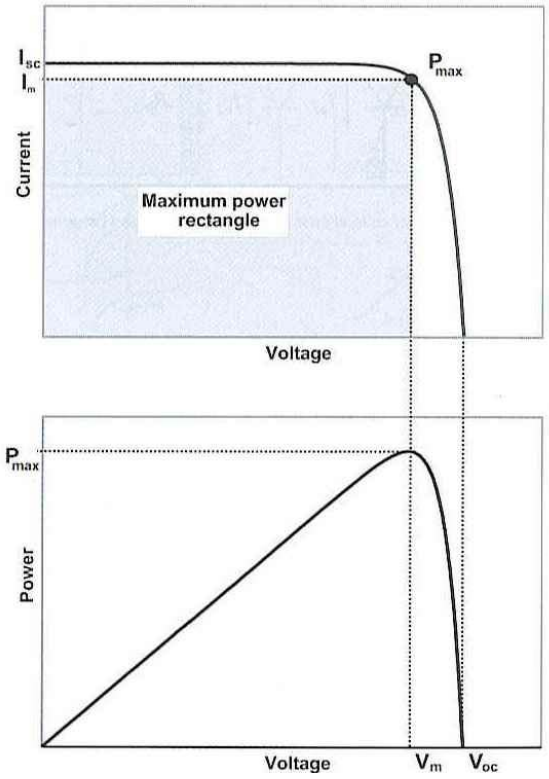

FIGURE 7-7: RELATION BETWEEN MAXIMUM POWER AND J_{SC} AND V_{OC} *[47]*

The I-V curve can be used to characterize the efficiency of a solar cell. As part of this plot it was mentioned previously the two characteristic points of the open circuit voltage (V_{OC}) and the short circuit current (J_{SC}). However, there are other important points such as the point where the solar cell has the maximum power ($P_{max} = I_{max} * V_{max}$). The ratio between the maximum power and the product of the V_{OC} and the J_{SC} is called the Fill Factor (FF) and it is a measure of the "squareness" of the curve (Equation 7-5 and Figure 7-7). The greater the fill factor (all other parameters being equal) implies greater conversion efficiency.

7.5.4. Efficiency

$$\eta = \frac{J_{SC} V_{OC} FF}{P_{in}}$$

EQUATION 7-6: EFFICIENCY EQUATION

Using these factors the efficiency "η" of the cell in gathering the incoming solar power (P_{in}) can be calculated. The relationship between these factors is shown in Equation 7-6. Some photovoltaic companies promote their devices only by mentioning the V_{OC} and the J_{SC} of their cells as benchmark parameters. This can lead to an overestimation of the actual efficiency of the device and the very important ratio of watts generated per dollar cost of the installed system.

8. Components of DSSC

The reference DSSC constructed for the research described here follow the basic elements introduced by Grätzel and his collaborators *[4]*. This project uses the reference cell design to test the efficiency of the novel improvements described in this research. The basic building blocks of DSSC are: conductive glass substrate, a TiO_2 layer as an electrode, a carbon layer as a counter-electrode, an organic dye to sensitize the electrode and generate photo-excited electron and an ionic liquid or electrolyte as a hole-transfer medium (Figure 8-1).

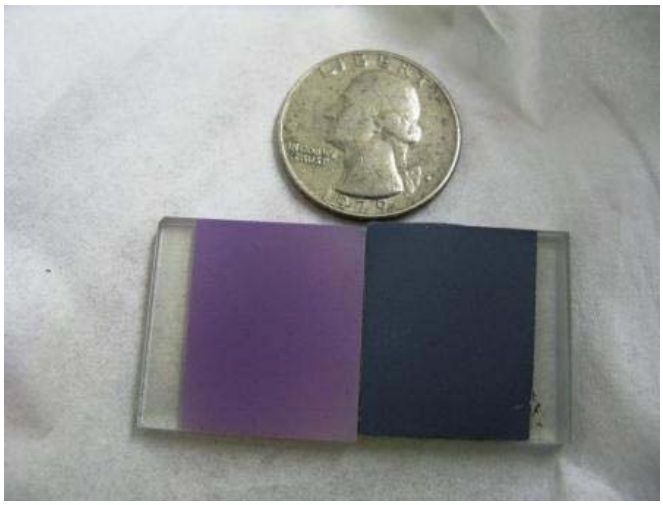

FIGURE 8-1: SIZE COMPARISON OF DSSC COMPONENTS

8.1. Substrate

The substrate is the base layer of DSSC. It obviously has to be optically transparent to accept the incoming light. It must also be conductive to act as a back contact for the photo-generated electrons. One of the most affordable choices for a substrate is glass coated with a thin conductive layer composed of Tin Oxide (TCO). Tin oxide is resilience to abrasion, has a low sheet resistance and it is optically transparent in the visible portion of the solar spectrum. TCO can withstand temperatures of up to ~450

to ~500 C that are necessary when annealing the other component layers and coatings *[58]*.

8.2. Electrode

The electrode has two major functions in DSSC:

- Forms a layer with an extremely high degree of porosity (surface area) where the sensitizer (Dye) is deposited.

- TiO_2 serves as a transport layer for the electrons injected into the layer from the dye sensitizer. This layer must transport electrons rapidly to the back-contacts so as to reduce recombination losses.

Researchers previously used monolithic surfaces of single crystal semiconductors as the electron conduction layer to which the dye molecules were attached. This presented a problem since the individual dye molecules absorbed less than 1% of the incoming light *[57]*. A clever solution is to use colloidal coatings of nano-crystalline titanium dioxide (TiO_2). The change from a flat interface layer to the highly porous TiO_2 matrix resulted in 1000 fold increase in the surface area available to the sensitizer for increased light harvesting and therefore greater generation of charge carriers *[4, 57]*.

TiO_2 (n-type material), has a conduction band that closely matches the excited energy level of organic dyes such as anthocyanins. Other materials including: ZnO, SnO_2, WO_2, $BaTiO_3$ have been investigated *[78]*. A close match energy levels is needed for the efficient injection of photo-excited electrons from the dye into the electrode and thus far TiO_2 appears to be the best option. TiO_2 shows a relatively small conductivity in its pure state. However, the conductivity increases under photo-generated electron injection. This photo-induced increase in the conductivity reduces ohmic losses significantly. Intentional doping the TiO_2 layer does not increase photovoltaic performance *[79]*.

TiO_2 has 3 phases (rutile, anatase and brookite) but the larger band gap of anatase (~3.2 eV) makes it more suitable for photovoltaics applications *[57]*. The electrode used in this work is composed of an annealed and sintered coating of titanium dioxide (anatase phase). The TiO_2 powder (P25, Degussa AG) used in this research consisted of TiO_2 nano-crystalline particles with particle sizes averaging around 25 nanometers.

Several research groups report the optimal TiO_2 film thickness to be ~ 10 um *[80, 81]*. These calculations have also shown a reduction of the V_{OC} as the thickness of the TiO2 layer increases. This has been explained as arising from a higher series resistance within the thicker TiO_2 layer. Thick film related losses may also be due to photoelectron concentration gradients *[82]*.

Caution must be taken when handling the TiO_2 powder since it tends to easily disperse into the air when disturbed or when transferred between containers. All powder mixing and handling was conducted within a fume hood by technicians wearing facemasks. Similar precautions were taken when handling the graphite powder used to make counter-electrode.

8.3. Counter-Electrode

The counter-electrode reduces the oxidized electrolyte (triiodide to iodide) so they can again replenish the electrons lost by the dye/sensitizer. It is important for the counter-electrode that it has a high electrocatalytic activity to reduce the electrolyte*[58]*. One of the elements that show the best performance as a counter-electrode is platinum *[83]*. However, the high cost of this material and its limited availability is a problem when considering low cost mass-manufacturing solar arrays *[57, 84]*. A suitable material that is both inexpensive and has a good catalytic activity is carbon *[84, 85]*. This became the material of choice used by this project.

Various carbon sources were investigated by this work. The first source of carbon used in this research originated from the soot produced during the combustion of a candle. This type of counter-electrode shows good performance despite being extremely fragile and susceptible to damage by contact or abrasion. Most of the DSSC educational demonstrations rely on this type of carbon coating due to its simplicity and its decent performance *[60]*. The first kind of counter-electrode that was investigated corresponds to this soot type. Initially these carbon coatings were created by coating the conductive substrates with the soot from a candle. Later counter-electrode samples were coated using a spray gun and graphite in solution.

Finally, as mentioned in the literature *[57]* coatings were created that are a mix of graphite powder and TiO_2. The optimum ratio between the components was around two parts of graphite per one part of TiO2 in weight. It is important to highlight the size difference between the particles. The average graphite particle size is 20 microns while the average particle size of the TiO_2 particles is 25 nanometers. The sintering of the mix at ~450 C creates a layer where the individual graphite particles are "cemented" in place within a matrix of TiO_2 particles.

8.4. Sensitizer

The sensitizer is the photo-sensitive material in DSSC's. It absorbs photons with energy equal or higher than the separation of low and high energy states present in the dye and then injects electrons into the electrode layer (TiO_2). The injection process needs to be extremely fast otherwise the photo-excited electrons would eventually decay back within the dye molecule or will be lost by recombination with the electrolyte. Other research groups reported that the lifetime for injection is in the femtosecond range while photoelectron decay to a states within the dye have lifetimes in range of microseconds *[86, 87]*.

One of the most important aspects to consider is contrast between the DSSC molecular electronic energy levels and semiconductor-based photovoltaics absorber materials that have an absorption band. The sensitizer in organic solar cells can have its absorption band tailored to a particular range. This opens the possibility of cells with multiple layers where dyes with a different absorption range can more efficiently harvest the solar spectrum.

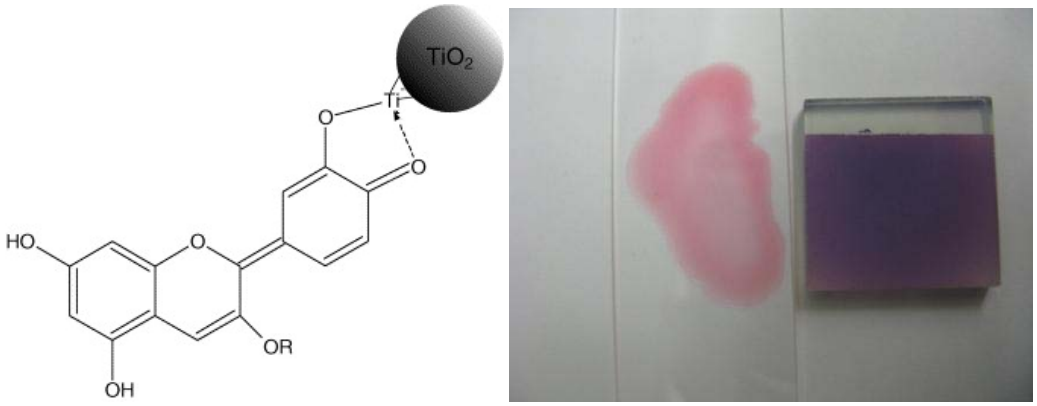

FIGURE 8-2: MOLECULAR STRUCTURE OF ANTHOCYANIN AND THE BINDING SITES TO TIO2 *[88]*(LEFT). COLORATION CHANGE OF DYE FROM AS EXTRACTED TO ABSORBED (RIGHT).

The UV-Vis absorption measurements were gathered using an "Evolution 300" UV/Vis spectrometer from Thermo-Scientific. This equipment was made available by Prof. Alexander Orlov at the Materials Science Department of Stony Brook University. During this measurement the dye was in a solution of water, methanol and acetic acid. Therefore a batch of these chemicals was mixed to serve as a reference. Then an absorption plot was taken that compares the spectra of the reference and the spectra of the dye in solution. The resulting plot shows only the contribution of extracted dye in the absorption of the light source as shown in Figure 8-3.

The dye that was selected for this project belongs to a type of flavonoid known as anthocyanins and was extracted and purified from California blackberries (Rubus ursinus). The extracted anthocyanins are responsible for the red and purple coloration in many fruits as in the case of blackberries *[67]*. Figure 8-2 shows the structure of anthocyanin molecule and its binding location with respect to TiO_2. The figure also

shows the location of the "=O" and "–OH" groups needed to chelate the dye molecule to the Ti^{IV} sites. Absorptions studies conducted in the UV-Vis spectra (shown below) reveal an absorption peak centered around ~ 513 nanometers (Figure 8-3). This figure also shows the absorption peak having a full width at half maximum (FWHM) of ~ 75 nanometers. This measured value correlates to values found in the literature *[67]*.

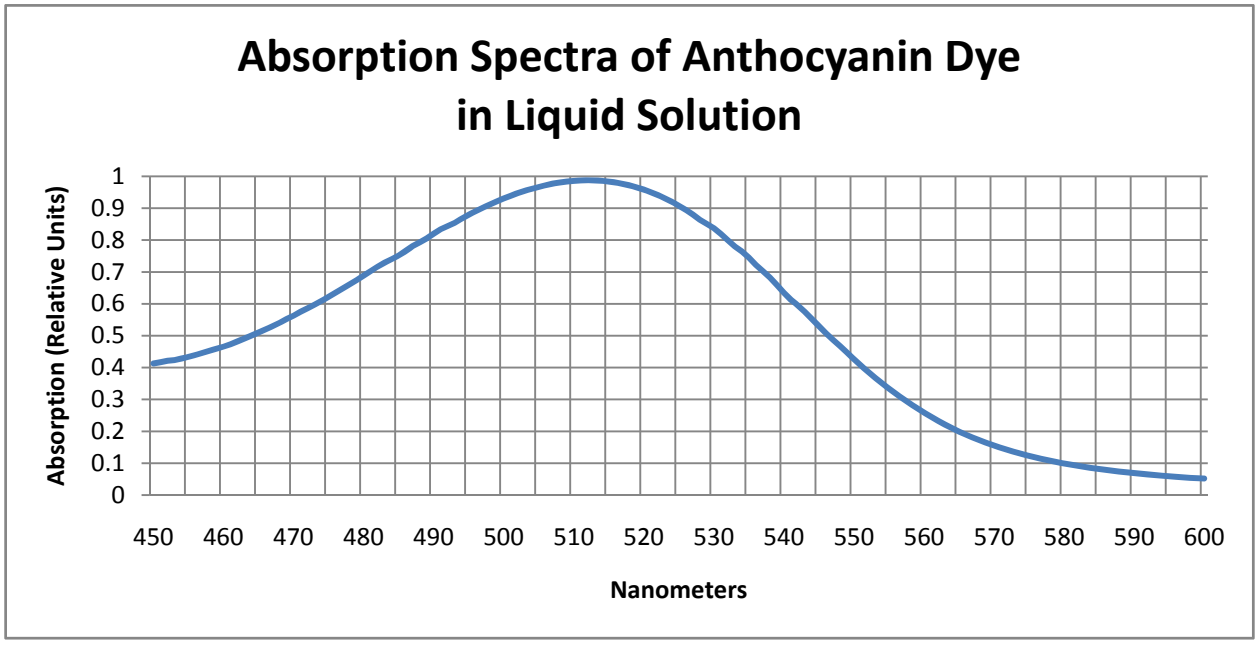

FIGURE 8-3. UV-VIS ABSORPTION SPECTRA OF EXTRACTED DYE.

It's trivial to find the separation between the HOMO and LUMO levels of the dye molecule using the gathered absorption spectra. This can be achieved by using the following approximation where λ is the absorption peak:

$$E_{Homo->Lumo} = \frac{1240}{\lambda}$$

EQUATION 8-1: SEPARATION BETWEEN HOMO AND LUMO STATES

Using the measured absorption peak of the extracted anthocyanin of 513 nanometers it is easy to calculate that the dye HOMO-LUMO separation is around 2.42 eV. This correlates with values found in the literature for the energy potential values of the HOMO and LUMO in anthocyanins *[61]*. It is important to note that the absorption

related electronic transition is greater than optimal for photovoltaic solar energy conversion (see e.g., Bube *[12]*)

8.5. Electrolyte

Typical ionic liquids used as electrolyte for DSSC consists of tri-iodide/ iodine in solution *[89]*. The solution was glycol alcohol. This redox couple is one of the most efficient electrolytes found; since, it closely matches the HOMO level of the anthocyanin dye. Also when used with a TiO_2 electrode it has a slow rate of reduction between the triiodide and the charges present in the TiO_2 particles thereby reducing recombination losses *[64]*. In summary the reaction rates between charges and the redox couple should be fast at the counter-electrode (carbon) and slow at the electrode (TiO_2) to reduce recombination losses *[62]*.

The iodide replenishes the charges lost by dye by oxidation and changes to triiodide. It travels towards the counter-electrode (carbon in this case) where it is reduced back to iodide by following route:

$$I_2^- + 2e^- \rightarrow 3I^-$$

EQUATION 8-2: IODIDE REDUCTION ROUTE

9. Construction of solar cells

The conductive glass substrates, nano-crystalline TiO_2 powder and electrolyte used in this project were purchased from the Institute of Chemical Education (I.C.E. at University of Wisconsin) as part of their "Nano-crystalline Solar Cell Kit". The purchase of these off-the-shelf kits was helpful in saving time since he alternative was to purchase individual components. It also enable this project to start investigations at a level where it was possible not only characterize DSSC with different construction parameters but also enabled investigations into novel optimization paths.

9.1. Preparation of substrates

The layers that make up a DSSC are deposited on top of transparent glass with a TCO coating containing tin oxide. The TCO layer is fairly resistant to abrasion and to the temperatures reached during annealing and sintering of the deposited electrode and counter-electrode coatings. The TiO_2 and carbon layers deposited on top of the TCO/glass substrate were annealed up to temperatures of ~500 C and ~450 C respectively without damage to the TCO.

The substrates must be handled, as carefully as is the case for optical device to avoid surfaces scratches. Before depositing either the TiO_2 or carbon coatings the glass substrates were placed inside a ultrasonic cleaner bath with the substrates immersed in a solution of 2-propanol alcohol for 5 minutes. After the cleaning cycle was completed the substrates were placed aside until all solvent evaporated.

9.2. Preparation of TiO_2 and C solution

The TiO_2 solution used to coat the electrode was prepared from a mix of TiO_2 powder (~25 nanometer average particle size) made by the Degussa company and a solution of deionized water, 2-propanol (laboratory grade from Fisher Scientific) and glacial acetic acid (99.9% made by J.T. Baker) in the ratio of 8ml/16ml/11ml respectively per gram of TiO_2 *[90]*.

Various solvents (ethanol and acetone) were tried at different ratios with deionized water with the optimal solvent being a mix of 2-propanol, acetic acid and deionized water. Acetic acid helps to decrease the series resistance of the TiO_2 layer and improves the absorption of the dye at the "=O" and "–OH" bonds present on surface of the TiO_2 particles *[70]*.

Three different techniques were used to deposit the counter-electrode carbon layer. First, the substrate was coated with the soot produced by a candle. Second, a carbon solution was prepared from a mix of graphite powder (Sigma Aldrich with an average particle size of ~20 um) and a solution of deionized water and 2-propanol (8ml/16ml respectively). Third, a more mechanically resilient counter-electrode layer, as previously mentioned by Graetzel *[57]*, was created composed of graphite and TiO_2 (2g/1g respectively) in a solution of deionized water and 2-propanol (8ml/16ml respectively). The added TiO_2 helps to bind the graphite particles and aids in the mechanical stability of the coating.

9.3. Deposition of electrode and counter-electrode layers

Different techniques were investigated to determine that capable of producing a uniform coating of TiO_2 or carbon. The properties and application of these techniques are the following:

9.3.1. Electrode

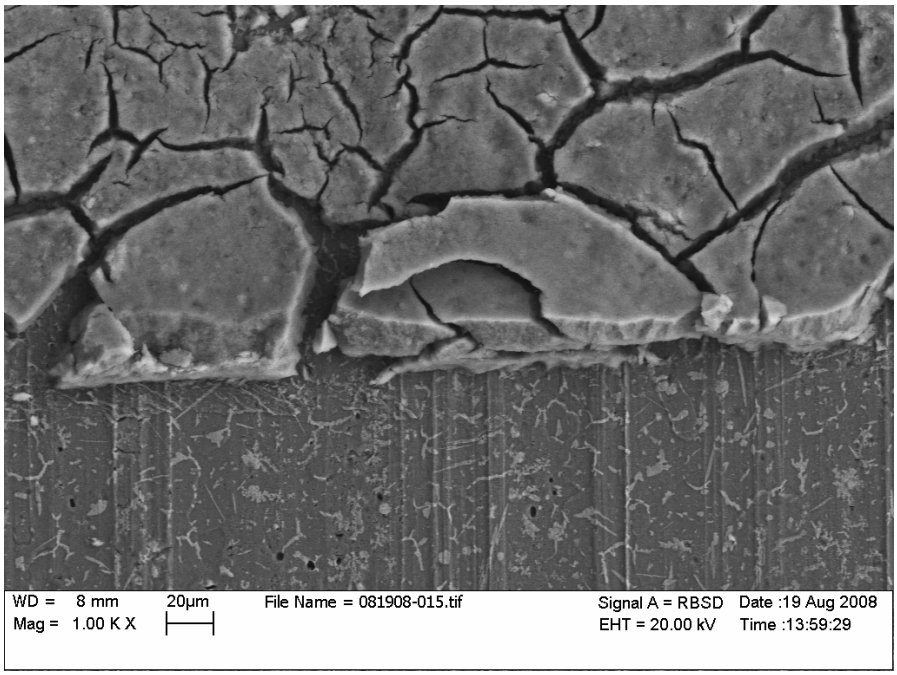

FIGURE 9-1: SEM IMAGE OF TIO2 COLD SPRAYED COATING

9.3.1.1. Doctor-blade technique (Mechanical application)

Initially TiO_2 layer was deposited using the "doctor blade" technique that has been used by other groups and is the most often method described in the DSSC literature *[57]*. This technique consists of creating a frame around the glass substrate that will control the thickness of the film (e.g., scotch tape) and then using a glass rod to spread the applied TiO_2 solution from one end of the frame and across the area to be coated.

However, after creating a number of coated substrates it was found that it was hard to control the uniformity and thickness of the deposited TiO_2 layer to the necessary level of precision. Since thickness and distribution depended on the amount of the solution initially deposited and the motion of the glass rod. This deposition technique usually resulted in a pooling of TiO_2 solution at the initial place of application with a non-uniform coating tapering off in thickness as the glass rod sweeps down the substrate.

9.3.1.2. Electro-spinning

This technique sought to deposit a high surface area TiO_2 coating using the electrospinning facilities of the SWING (Stem cell, Wound healing, Inflamation and Nanotechnology Group) center *[91]*. The electrospinning setup consisted of a syringe containing the material to be deposited and a mounting plate that holding the target to be coated. The target and syringe are connected to a voltage source that creates an electro-potential difference between the syringe and the mounting plate in the range of 1000 volts. When the solution inside the syringe is slowly pumped out, the solution will be propelled with great speed towards the target due to the electric field.

A matrix of interlaced filaments has also been used involving a suitable polymer mixed with the material to be deposited and subsequently annealed to burn out the polymer. This work examined the possibility that deposited layers of interconnected TiO_2 filaments using this technique would have a high surface area and porosity. This technique was hoped to produce high surface area and porosity coatings as to increase the amounts of dye deposited on the TiO_2 surface as in the case of the nano-particles.

Initial results were encouraging with J_{SC} and V_{OC} values greater than what was initially achieved using the "doctor-blade technique". However, after experimenting with the setup it was realized that the thickness of the coating had a radial distribution. It was thicker at the point where the needle of the syringe was aimed with thinning as the radial displacement increased. This problem arises because the material propelled from the syringe disperses into a cone shaped plume while in flight. It would have been possible to correct this problem by building an apparatus to raster scan the syringe over the target but it was not possible to modify the existing setup within the timeframe of this work.

9.3.1.3. Screen printing

After working with the previous techniques the most important problem that had to be solved was the non-uniformity in the thickness of coatings. Note some commercial

companies*[42, 43]* have developed industrial-scale fabrication lines for organic solar cells. The production technique used to manufacture these cells was based on extruding a TiO_2 solution through a mesh with pore sizes of very small diameter. The TiO_2 is forced through a mesh by the application of force through a squeegee.

This technique has not only been used with the manufacturing of organic solar cells but it has also been tested with other kinds of photovoltaics as done by the Japanese company Matshushita with thin-film CdTe solar cells *[44]*. Some of the benefits from this technique are the simplicity of the procedure, the ability to deposit a TiO_2 layer on an array of substrates at the same time and the ability to print all the elements of a DSSC layer by layer.

A screen printing kit (Toolkit - Screen Printing Kit by Speeball) was purchased to test the feasibility of applying this technique to the DSSC studied in this research. The TiO_2 solution was mixed in the same manner as it was used for the doctor-blade technique. The TiO_2 was applied to the surface of the mesh that was placed securely on top of the conductive side of the glass substrate. The supplied squeegee was used to smoothly drive the TiO_2 through the mesh. However, it was noticed that after applying the TiO_2 solution the mesh did no separate smoothly from the substrate. This may arise from the surface tension created by the TiO_2 solution binding the surface of the substrate and the mesh. This problem can be visualized by imagining what happens when an object is pulled out from the surface of a viscous material. After the object has been removed a protrusion is left on the surface that will slowly subside down depending on the viscosity of the material (example: Honey and a spoon). The final result was that this TiO_2 deposition produced layers with high surface roughness (millimeters).

9.3.1.4. Cold spraying

The final technique that produced the most consistent results is a variation of a deposition process that has been used previously by others *[45, 92]*. This technique consists of painting the surface of the conductive substrate with an air-brush. This

research used an inexpensive air spraying kit purchased from a hobby shop. The spraying hardware consists of a gun with a nozzle that shoots out the TiO_2 solution that is propelled with the compressed air. The amount of air coming from the nozzle can be controlled and this controls the rate of flow of the solution coming out from the nozzle.

An important factor to be considered is the ratio of the solvents (e.g. 2-propanol) versus the material to be deposited (e.g. TiO_2 or carbon). The solution to be deposited exits the nozzle of the gun in the form of tiny droplets. Solvents present in the solution evaporate as the droplets travel towards the target. Therefore, the amount of the solvents in the solution (TiO_2) must be increase in order to avoid the agglomeration of the particles as they reach the target surface as compared to the "doctor-blade" technique.

The coatings that were deposited using the spray technique have been analyzed with the help of a scanning electron microscope and have been found to have a thickness in the order of ~10 microns (Figure 9-1). Research done by other groups have found this thickness of TiO_2 used as an electrode to maximize the efficiency of DSSC *[80]*.

9.3.2. Counter-electrode

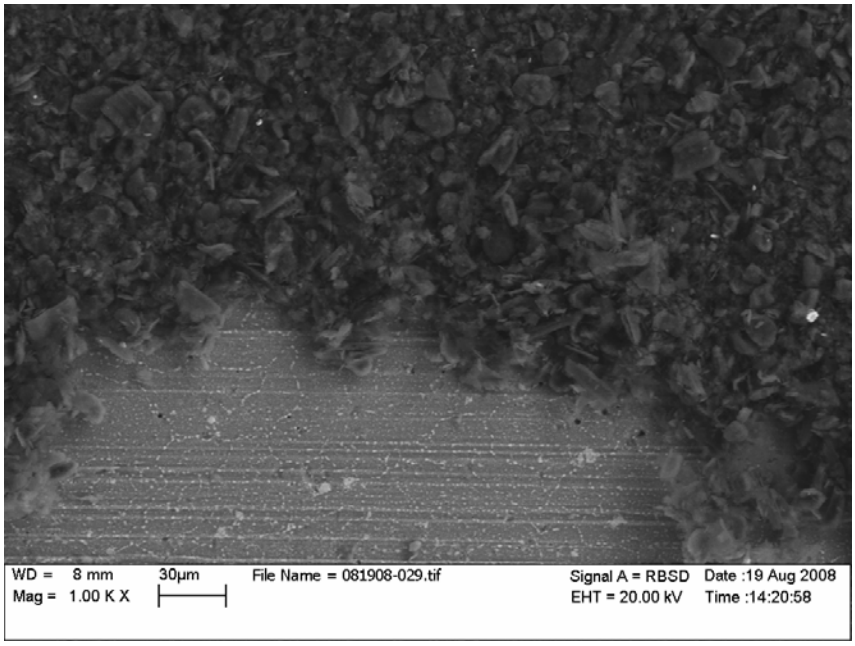

FIGURE 9-2: SEM IMAGE OF CARBON (GRAPHITE) COLD SPRAYED COATING

9.3.2.1. Soot

The first technique that was used to create the carbon counter-electrode layer was to simply deposit the soot produced through combustion from a candle onto the surface of the conductive glass substrate *[60]*. This process is extremely simple and it is used for the construction of demonstration DSSC. The photovoltaic efficiency of DSSC produced using this type of carbon deposition shows good results compared to other deposition techniques. This is due to the small particles of carbon produced during combustion that studies have found to be as small as 10 nanometers *[93]*. The small particle size has a large surface area available for the catalytic conversion of tri-iodide back to iodide.

The main problem from this carbon deposition technique is that the carbon coatings deposited are extremely fragile. Handling of the coated substrates must be careful since just touching the surface can damage the coating. It was discovered that after the DSSC has been assembled and the electrolyte placed between the plates the soot/carbon coating tends to disperse inside the cell. This is because the electrolyte is inserted into the device by applying drops of the liquid at the interface between the electrode and counter-electrode substrates. The liquid is driven inside the cell by surface tension. This process appears to wash soot/carbon into the electrolyte.

9.3.2.2. Cold spraying

The cold spraying technique previously used for the electrode was finally used to deposit the carbon layer as it proved to produce uniform TiO_2 coatings. Graphite powder was purchased from Sigma-Aldrich (SN: 282863) with a particle size of less than 20 microns. Two different types of carbon counter-electrode solutions were created. The first type is a mix of carbon and TiO_2 (2g/1g respectively) in a solution of deionized water and 2-propanol (8ml/16ml respectively). The second type used the same quantity and ratio of solvents but without TiO_2. Tests were done comparing the efficiency between the two types counter-electrode solution which will be shown in following chapters. After

spraying the samples were left to dry for 30 minutes and then were annealed in a temperature controlled furnace. The annealed counter-electrode coating can be seen in Figure 9-2.

9.4. Annealing and Sintering of the deposited layers

The electron and counter-electrode coatings were annealed in order to harden and sinter the coatings. This process was carried at the Magnetic Materials Laboratory of Prof. Richard Gambino at the Stony Brook Materials Science department. It's important to anneal the coatings to evaporate water and moisture trapped inside the coating. The annealing temperature is not high enough to change the phase of the TiO_2 nano-particles (anatase) used in the coatings. The high temperature also sinters the particles at their connection points *[57]*. This connection helps the electrons encounter a continuous path as they travel from their photo-excitation sites at the dye molecules, through the TiO_2 layer until they finally encounter the TCO back contacts on the glass substrate.

The standard annealing temperatures for the electrodes was set at ~500 C *[90]*and ~450 C *[85]*for the counter-electrodes. Studies on the relation between temperature and efficiency were carried out comparing the effects of low annealing temperature and the output of the devices. The results will be show in the following experimental results section. It is possible that the TCO (Tin Oxide) on the surface of the substrates could deteriorate after repeated annealing cycles at high temperature. However, the performance of the DSSC decreases as the annealing temperature of the TiO_2 coating decreases.

9.5. Extraction and Purification of Dye

In the DSSC that were studied in this research the dye or sensitizer is anthocyanin that was extracted and purified from California blackberries (Rubus ursinus). This dye was selected based in the need to have a dye that was affordable and that doesn't have

any toxicity when handled. Also, most inorganic dyes used as sensitizers are costly and current work being done on organic dyes shows their potential to create efficient organic photovoltaics *[94, 95]*.

The liquid extracted from blackberries has a dark red/purple coloration and contains the anthocyanin dye as well as multiple organic components and water. The dye was purified and separated by mixing the extracted juice with methanol, water and acetic acid in a ratio of 20/25/5 ml *[67]*. The solution was left to rest for a few hours until all the solid and liquid materials have separated within the column. The middle third of the column was then extracted as it has shown to contain the highest concentration of the anthocyanins useful as dye or sensitizer in DSSC *[67]*.

9.6. Absorption of dye on TiO_2 substrate

The glass substrates with the deposited and annealed TiO_2 coatings are placed inside a bath of the purified dye for a period of up to an hour. Tests were conducted to see whether prolonged submersion (up to two days) improved the behavior of the DSSC. It was found that 1 hour was the optimal time staining time for the TiO_2 coating. Once the dye is in contact with the surface of the TiO_2 layer it stains it with a dark purple color (Figure 8-1 and Figure 8-2). The dye molecules are not trapped inside the TiO_2 matrix but form complexes with the surface of the individual particles. The porosity of the deposited film makes it possible for the dye to coat not only the external surface of the coating but also the particles embedded inside the matrix. The dye forms a coating with a monolayer thickness around the TiO_2 particles.

The charge transfer process between dye-TiO_2 is ligand-centered and it's mediated by the "=O" and "-OH" sites present on the surface of the TiO_2 particles where the dye molecules are attached. Extracted dye as shown in Figure 8-3 has a broad absorption peak centered between 450 to 550 nanometers. However, upon its attachment to the TiO_2 the absorption spectrum of the dye shifts towards the blue as visually seen in

Figure 8-2 on the right side. This shift is due to the structure change of anthocyanin from the quinoidal to flavilium form *[96]*.

After the TiO_2 coated substrates have been stained they are cleaned first with deionized water and then rinsed with ethanol as to remove any leftover water trapped inside the coatings. They are left to dry for around 15 minutes before being integrated into the DSSC.

9.7. Integration of elements and addition of the electrolyte

The final step in the construction of the DSSC is the integration of the previously prepared components. The electrode and counter-electrode substrates are placed together with an offset as to let the uncoated areas in the conductive sides of the substrates available as electrical back contacts. The substrates are held together using mounting clips positioned close to the edges as to let the maximum amount of light inside the cell. Finally, drops of the iodine electrolyte are applied to the interface between the substrates while surface tension drives the electrolyte inside the cell. It will take around 15 minutes for the electrolyte to completely coat the interface between the electrode and counter-electrode. After the electrolyte has completely coated the interior of the cell and the back contacts have been cleaned of any leftover electrolyte the cells are ready for testing.

10.Experimental Details

Starting with standard Gratzel [2-4] type DSSC parameters were explored and hypothesis tested to better determine molecular level descriptions and optimize photovoltaic performance. In particular by systematically varying parameters that control: various charge transport mechanisms, optical absorption, contacting, etc. it is possible to begin to understand the relationship among these, material processing technique, and solar cell performance. Finally, tests were done on the resilience of DSSC against weathering.

10.1. I-V Curves of DSSC of different parameters

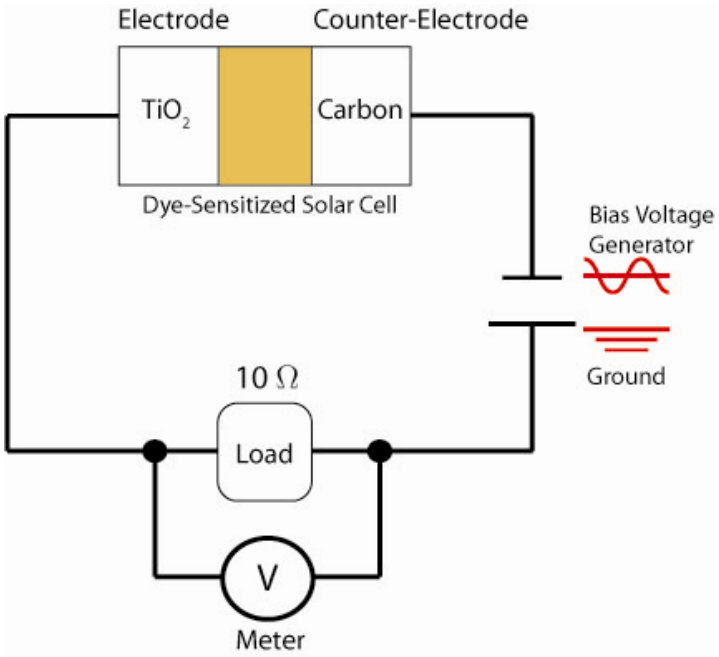

FIGURE 10-1: DIAGRAM OF CUSTOM MADE SETUP USED TO PLOT IV CURVES OF OUR DEVICES

For this research a custom made automated photovoltaics test-bench recorded I-V curves was developed and employed. The components of the test-bench are shown in Figure 10-1. The signal generator (ScienceWorkshop 750 USB Data Logger) and a variable load (Potentiometer) were used here. The signal generator creates a ramp-up

voltage to bias the cell while the photocurrent is measured indirectly by recording the voltage drop across a known load provided by the potentiometer. Cell voltage and the applied bias were recorded by the data logger and the resultant I-V curves plotted.

10.1.1. Effect of deposition technique (electrode)

It is important to compare if there were improvements on the photovoltaic efficiency of the DSSC between the "doctor-blade" and spray method. As shown in Figure 10-2 the newly develop air-spray technique shows a clear improvement over the more commonly used "doctor-blade" type of TiO_2 application. Air-sprayed DSSC show definite improvement in key photovoltaic parameters as quantified in Figure 10-2.

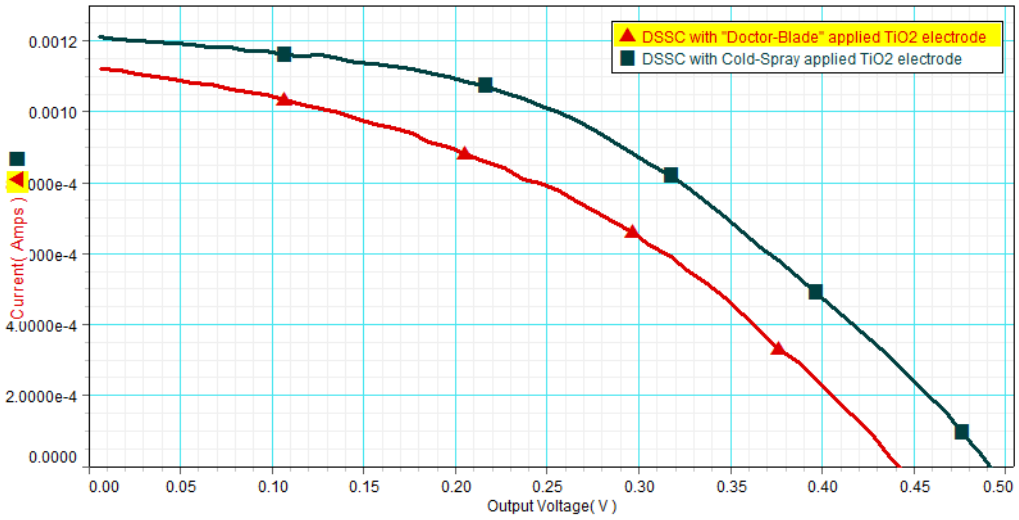

FIGURE 10-2: COMPARISON BETWEEN TIO2 APPLICATION METHODS (DOCTOR BLADE AND AIR-SPRAY) VS. EFFICIENCY

The improvement in V_{OC} and J_{SC} of the air-sprayed cell can be related to the decrease in R_{Series} as shown in Table 1. This decrease in resistance may be mediated by the reduction in overall thickness of the TiO_2 layer, better adhesion and/or better electrical contact to the substrate. As mentioned previously the conductivity of TiO_2 is influenced by the density of injected electrons and thick films may generate electron concentration gradients sufficient to affect electronic transport.

The "doctor-blade" application of TiO_2 can result in coatings of variable thickness and some films peeled off during drying and annealing. Peeling leaves regions of the TCO layer in direct contact with the electrolyte; a current leakage path that results in decreased open circuit voltage.

The reduction in recombination losses can also be seen in the increase of the experimental R_{Shunt} value for the air-spray cells as shown in Table 1. The optimum film thickness has been found to be around 10 micrometers using numerical and experimental calculations as previously reported *[80, 90]*. Using the spray deposition method it was possible to create thin TiO_2 coatings as shown using electron microscopy in Figure 9-1.

Technique	**V_{OC} (V)**	**J_{SC} (mA)**	**V_{Max} (V)**	**J_{Max} (mA)**	**R_{Shunt} (Ohms)**	**R_{Series} (Ohms)**	**Fill Factor**
Doctor Blade	0.442	1.13	0.261	0.77	1100	270→120	0.4
Air-Spray	0.49	1.22	0.296	0.9	1800	250→90	0.45

TABLE 1: PARAMETERS OF DSSC WITH DIFFERENT ELECTRODE APPLICATION

During this work it was not possible to successfully develop a screen printing apparatus that produced solar cells as efficient as the spray method. Significantly, the cold-spray method like screen-printing can easily be scaled-up to industrial sizes and throughput.

10.1.2. Effect of deposition technique (counter-electrode)

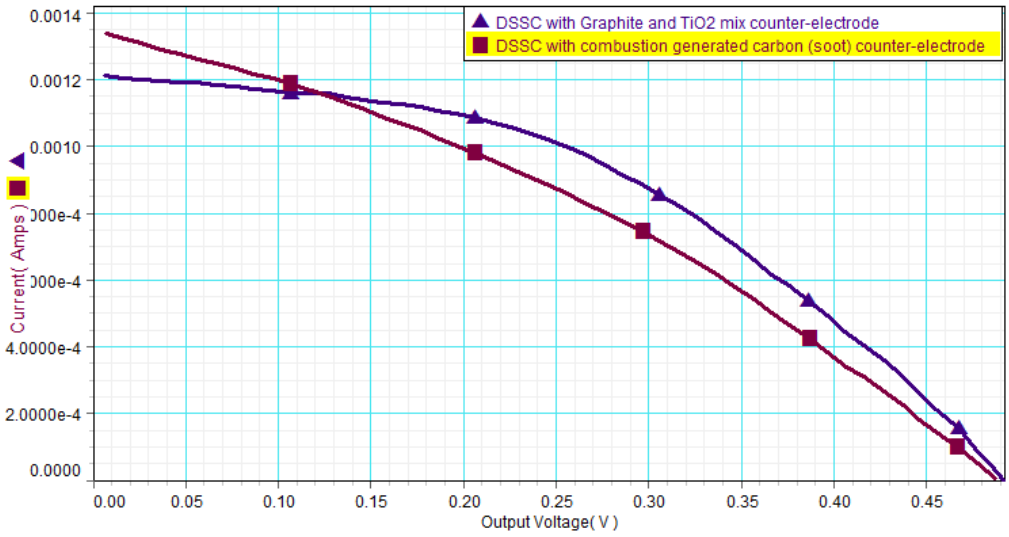

FIGURE 10-3: COMPARISON BETWEEN DIFFERENT ORIGIN CARBON COUNTER-ELECTRODE COATINGS (SOOT AND GRAPHITE) VS. EFFICIENCY

Various preparation techniques and coatings were used to determine the optimum process to create counter-electrodes. DSSC with counter-electrode containing carbon from soot and graphite were compared. The I-V curves of two types of counter-electrode are shown in Figure 10-3. The higher J_{SC} of the DSSC using soot appears to arises from the much smaller particle size (10 nanometers) *[93]* as compared to the 25 microns particle size of the graphite particles used with the spray. Smaller particle size leads to an increase in the surface area available for catalytic conversion of the redox couple electrolyte. In-turn this may lead to an increase in the rate of reduction of the dye molecules. Therefore, increase of the counter-electrode surface area may translate to an increase in the flux of charges across the DSSC.

Carbon Source	V_{OC} (V)	J_{SC} (mA)	V_{Max} (V)	J_{Max} (mA)	R_{Shunt} (Ohms)	R_{Series} (Ohms)	Fill Factor
Soot (Nano particles)	0.487	1.34	0.276	0.8	600	300→200	0.34
Graphite/TiO2 (Micro Particles)	0.49	1.22	0.296	0.9	2300	250→90	0.45

TABLE 2: PARAMETERS OF DSSC WITH CARBON COUNTER-ELECTRODES MADE FROM DIFFERENT SOURCES.

However, as shown in Figure 10-3 and Table 2 the soot counter-electrode exhibits a performance reduction in other photovoltaics parameters. The soot containing DSSC has a detrimental decrease in the values of R_{Shunt} and an increase in R_{Series}. As mentioned previously the soot coating tends to separate from the substrate and mix with the electrolyte. This will cause an increase in recombination losses between the electrolyte and the bare areas of the counter-electrode substrate leading to a decrease in R_{Shunt}. The soot particles suspended in the electrolyte may also leads to an increase in the R_{Series} of the liquid medium. It should be noted that despite these problems the V_{OC} value is similar between the soot and graphite counter-electrode cells despite. Greater recombination losses lead to a decrease in V_{OC} and the soot cell could be capable of producing a larger photovoltage than the standard cell. It's foreseen that correcting issues such as recombination at the back contact and separation of the soot could lead to better performance in general for DSSC containing carbon nano-particle counter-electrodes.

10.1.3. Effect of annealing temperature

Temperature	V_{OC} (V)	J_{SC} (mA)	V_{Max} (V)	J_{Max} (mA)	R_{Shunt} (Ohms)	R_{Series} (Ohms)	Fill Factor
Electrode at 300C	0.255	0.14	0.160	0.08	3200	1570→700	0.40
Counter-electrode at 300C	0.470	0.59	0.337	0.41	3600	680→390	0.50
Normal Annealing	0.490	1.22	0.296	0.9	2300	250→90	0.45

TABLE 3: PARAMETERS OF DSSC WITH VARIATIONS IN ELECTRODE AND COUNTER-ELECTRODE ANNEALING TIME

The TiO_2 annealing temperature dependence of the DSSC performance was investigated. A relatively high annealing temperature (~500 C) is needed to properly sinter TiO_2 particles for the proper conduction of injected electrons. However, lower

annealing temperatures may be desired in applications where the substrate is temperature sensitive (i.e. flexible photovoltaics in polymer substrates). Figure 10-4 and Table 3 shows the effect of annealing temperature for both the electrode and counter-electrode cases as compared to a standard annealing temperature DSSC. The changes due to the lowered annealing temperature are dramatic and show a marked reduction in performance.

In the case of the TiO_2 electrode it is known that at lower annealing temperatures nano-particles do no sinter; therefore, electrical contact between individual particles is incomplete or absent *[97]*. This causes the injected electrons to be trapped inside the particles until they recombine with the electrolyte. This leads to a performance reduction in all key photovoltaic parameters but especially in the photocurrent and photovoltage.

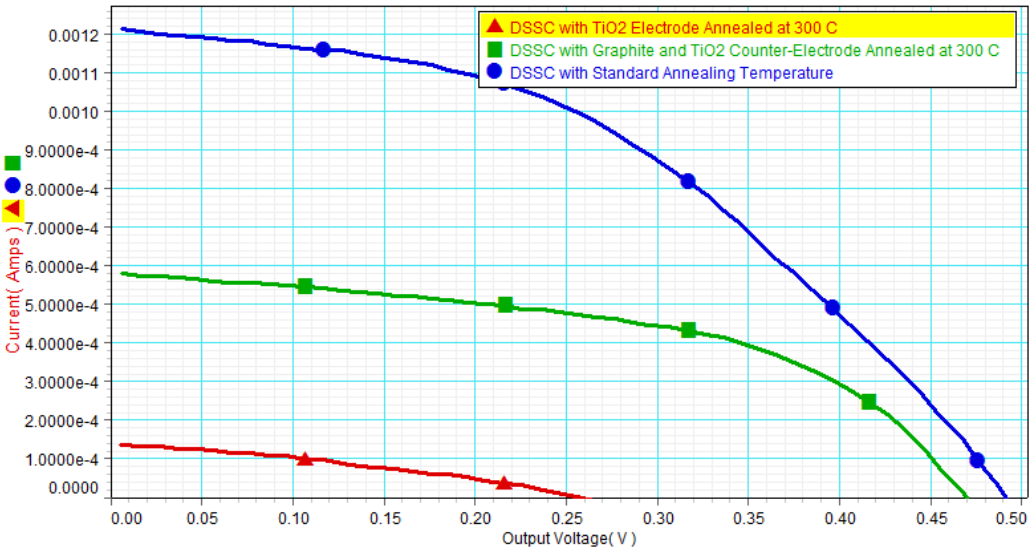

FIGURE 10-4: COMPARISON BETWEEN ANNEALING TEMPERATURE (ELECTRODE AND COUNTER-ELECTRODE) VS. EFFICIENCY

In the case of the graphite/TiO_2 counter-electrode the reduction in performance due to low annealing temperature is not as dramatic as in the case of the electrode. The graphite particles (~ 20 microns) are 1000 times larger than the TiO_2 particles. As observed using an electron microscope in Figure 9-2 the coating is essentially a particle monolayer. Therefore, inter-particle charge conduction is not an issue. However, the graphite to TCO charge transfer may be reduced due to a lack of atomic level bonding at

the lower annealing temperatures. This leads to a decrease in the photovoltage and photocurrent by the reduction of charge transfer through the electrolyte and recombination losses of trapped charges in the counter-electrode layer.

10.1.4. Effect of counter-electrode composition

Different counter-electrode with a mix of graphite and TiO_2 were tested to determine a ratio that would improve the performance of the DSSC as compared to the reference Graetzel cell (pure graphite) used here. As mentioned previously Graetzel introduced the idea of creating mixed carbon and TiO_2 counter-electrodes *[57]*. The addition of TiO_2 aids in the mechanical resilience of the graphite coating and may improve the charge transfer between graphite particles and the TCO.

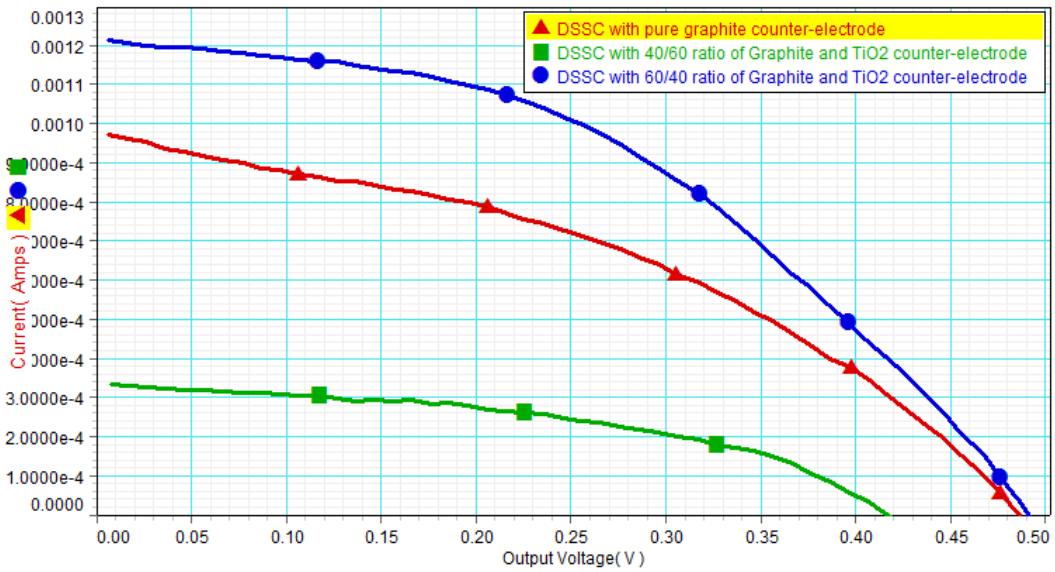

FIGURE 10-5: COMPARISON BETWEEN COMPOSITIONS OF THE COUNTER-ELECTRODE (RATIO OF TIO2/GRAPHITE) VS. EFFICIENCY

This research has shown that the addition of TiO_2 may cause an increase or decrease in the DSSC performance depending on the graphite/TiO_2 ratio. Electron microscope examination of the mixed counter electrodes used here found that the graphite particles are isolated on top of the substrate due to their relative large size (~20

microns) with respect to the coating thickness (Figure 9-2). Therefore, the surface remains essentially carbon particle in nature. It can be concluded that the addition of TiO results in the formation of a conductive matrix that not only helps hold the graphite particles in place but may also provide a medium for the charge transfer process between the TCO and the graphite particles.

As shown in Figure 10-5 and Table 4 the optimum ratio was found to be around 60% graphite and 40% TiO_2 per weight. This particular ratio shows an increase in R_{Shunt} due to better coverage leaving less TCO exposed to the electrolyte. This leads to a reduction in recombination losses at the counter-electrode and an increase of both V_{OC} and J_{SC} with respect to a standard pure graphite counter-electrode. The higher J_{SC} shown by this mix can be related to the improved charge transfer between the electrolyte and the graphite. This will subsequently increase the amount of reduced electrolyte (iodide) able to in-turn reduce the dye thereby completing the photo-excitation and injection cycle more quickly.

Composition	V_{OC} (V)	J_{SC} (mA)	V_{Max} (V)	J_{Max} (mA)	R_{Shunt} (Ohms)	R_{Series} (Ohms)	Fill Factor
Pure graphite	0.485	0.98	0.290	0.64	900	380→220	0.39
60/40 Mix TiO2/Graphite	0.415	0.335	0.270	0.235	3448	890→370	0.46
40/60 Mix TiO2/Graphite	0.490	1.22	0.296	0.9	2300	250→90	0.45

TABLE 4: PARAMETERS OF DSSC WITH VARIATIONS IN THE GRAPHITE CONCENTRATION OF THE COUNTER-ELECTRODE

A counter-electrode mix with a higher concentration of TiO_2 was also tested (60% TiO_2 and 40% graphite per weight). It was found that higher TiO_2 concentration reduced the performance of the cell. This can be easily explained as being due to the decreased graphite surface area able to catalytically cycle the electrolyte from its oxidized (triiodide) to its reduced (iodide) form.

10.2. Quantum Efficiency (Q.E.) Measurements

For efficient harvesting of solar energy it is indispensable to have a solar cell that can absorb as much of the solar spectrum with matching device peak absorbance and solar peak emission. The following quantum efficiency measurement shows the wavelength depending absorption and power generation of the DSSC. The measurements were recorded using a Newport "Cornerstone 260" mono-chromator and a mercury-xenon 600 watts arc lamp (Prof. Orlov facilities) *[98]*.

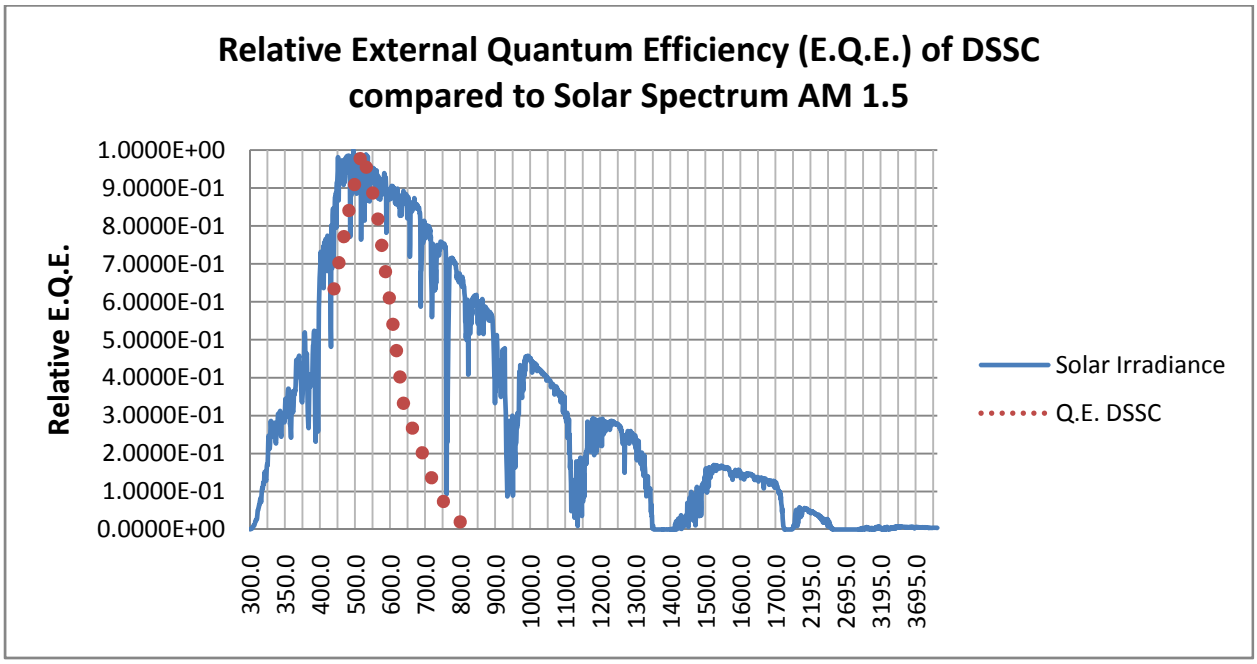

FIGURE 10-6: COMPARISSON OF MEASURED Q.E. WITH SOLAR IRRADIANCE AT AM 1.5 CONDITIONS

The results presented in Figure 10-6 show a comparison between the evaluated Q.E. of DSSC's and the standard A.M. 1.5 solar irradiance reporting conditions *[99]*. The values were normalized as to show the relative peak DSSC absorption and solar emission. The results presented in Figure 10-6 show that the DSSC that was tested its most efficient at ~520 nanometers. The efficiency maximum is also close to the spectral region where most of the solar energy is contained. It should be noted that the spectral resolution of the mono-chromator is 20 nanometers and that this value determines the uncertainty in the measurements.

The measured quantum efficiency of the DSSC containing anthocyanin dye shows a favorably spectral absorption peak with respect to the solar spectrum. This result verifies the prospect of using dyes derived from nature as an affordable light absorbing and charge carriers generating material for DSSC's. However, as it can be seen in Figure 10-6 the spectral absorption of the dye is narrow and most of the long wavelength (>500 nanometers) solar energy is not absorbed and will not contribute to electrical power generation. Alternatives have been explored that use tandem DSSC that uses stacked layers that efficiently absorb different parts of the solar spectrum *[27, 100]*.

10.3. Comparison of Dye in solution and adsorbed on TiO_2

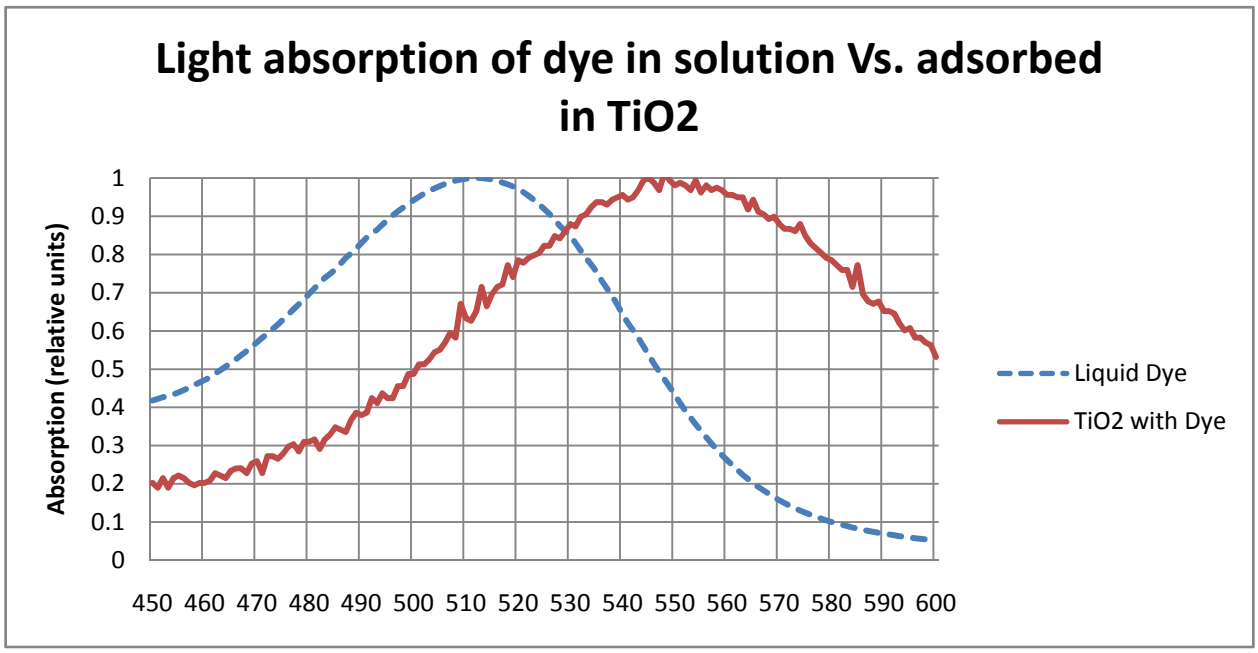

FIGURE 10-7: LIGHT ABSORPTION OF DYE IN LIQUID SOLUTION AND ADSORBED BY TIO2

Research was done on the changes in the absorption spectrum of anthocyanin dyes from as extracted (liquid solution) and after it has been adsorbed by the TiO_2 layer. In one sample, the extracted dye was diluted with deionized water while in the second one the non-diluted dye was adsorbed on an annealed coating of TiO_2. In this

experiment an UV/Vis absorption spectrometer “Evolution 300” from Thermo-Scienctific was used to record the data (Prof.Orlov facilities).

The gathered results are presented in Figure 10-7 and show a light absorption shift to the red by TiO_2 + Dye sample. This change in the absorption by anthocyanin has been documented previously in the literature *[67]*. It has been explained as arising from the complexation mechanism between the dye molecule and the surface of the TiO_2 nano particles (and other metal ions) *[101]*. The dye-TiO_2 adsorbtion causes a shift from the flavilium to the quinonoidal form of anthocyan that has a purple-blue coloration as seen in Figure 8-2 *[67]*. Studies have also indicated that these changes also lead to a shift between the relative separation and position of the LUMO and HOMO levels of the dye. This change shifted the absorption peak of the dye from ~512 nanometers in solution to ~547 nanometers when adsorbed to TiO_2.

It should be noted that the light absorption peak of the dye adsorbed on TiO_2 does not match the measured quantum efficiency peak as a function of the wavelenght ($\Delta \approx 27$ nanometers). This can be explained by the different conditions sorrounding the dye molecule. In the Q.E. the molecule was sorrounded by the liquid electroly while in the light absorption test the dye molecule was on top of a dry TiO_2 substrate and exposed to air. It has been suggested that the medium (e.g., water or air) has an influence on the electronic properties of the dye *[102]*. The presence of a liquid medium sorrounding the dye can be responsible for shifts in the HOMO-LUMO separation that leads to the observed discrepancies in the wavelenght dependend quantum efficiency and light absorption.

10.4. Environmental Effects

Testing has been done on the environmental resilience of the DSSCs studied in this research. The testing setup used in this experiment consisted of a portable voltage data logger (USB-503 from Measurement Computing) connected to an array of four DSSCs

connected in series. The array was left overnight beneath a glass hemisphere located outdoors. The glass hemisphere protected the electrical contacts from wind and rain while letting through light unimpeded. The effect of the day/night cycle (4:40PM → 12:00 PM) on the voltage output the DSSC can be seen in Figure 10-8. From the data recorded the following conclusions can be stated:

- The voltage output was at its highest at the start of the test even when the test was initiated past noon (4:40PM). The high voltage is due the series connection of four cells. It is noteworthy that some degradation is occurring as the highest voltage was recorded at the beginning (~1.4 volts) of the test which was under a much lower irradiance than the following morning which produced a Voc of only 0.7 Volts before the electrolyte dried up. It should be mentioned that the individual cells produced an individual V_{OC} of ~450 Volts while illuminated by the sun at noon right after being assembled.

- The recorded voltage drops fast during the sunset and as expected is below detection limits at night.

- The voltage rises again during the morning but it reaches a plateau (~0.7 volts) and then starts falling down at around 8:00 AM. These declines were correlated with a slow loss of the electrolyte over night and rapid dye evaporation during the morning heating. Electrolyte loss can easily prevented by a more robust seal between the two glass substrates used to prepare these cells. A limited investigation of sealants was conducted in this work.

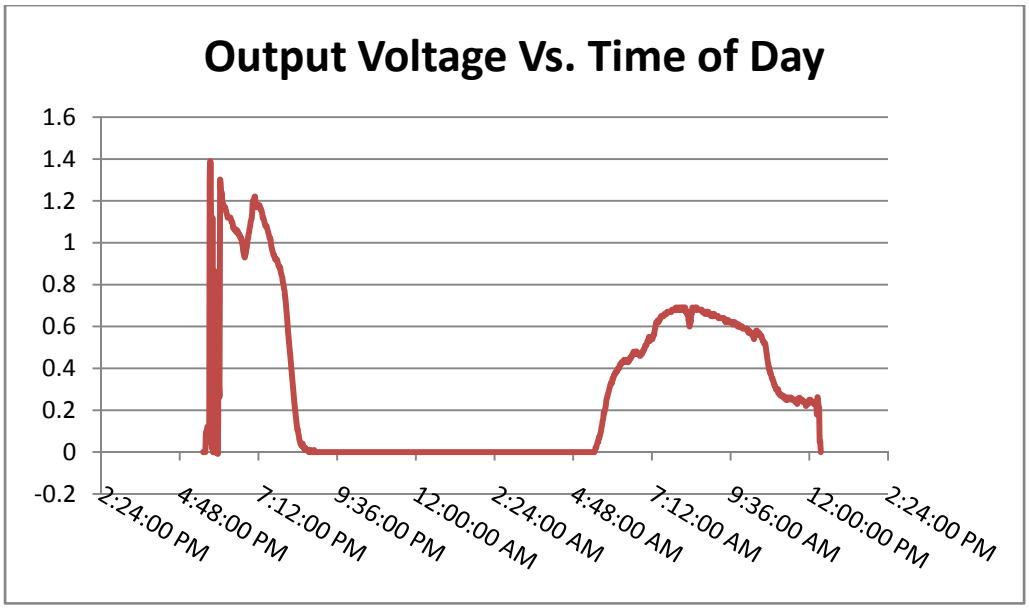

FIGURE 10-8: EFFECT OF THE DAY-NIGHT CYCLE ON THE VOLTAGE OUTPUT OF AN ARRAY OF DSSC'S

The most important short term problem on the environmental survivability of DSSCs is the loss of electrolyte. The first solution considered was the application of a commercial silicone sealing compound around the edges of the cell. However, the silicone sealant used proved unable to prevent the leakage of the liquid electrolyte. Also, the sealant could be porous enough to provide a path for the escape of vapors from the electrolyte. Other materials such as glass-frit or Surlyn ^{tm} (ionomer thermoplastic made by DuPont) have been successfully used as an encapsulation material for organic solar cells by other groups *[103]*.

An apparatus to melt the glass-frit and encapsulate the DSSC is currently being designed. However, this type of encapsulant poses problems to the stability of the organic dye used in this research due to the high processing temperature needed to melt the glass. The electrolyte also needs to be inserted into the device after the encapsulation process. Therefore, entry channels for the dye/electrolyte must be drilled into the device as done by other research groups *[104, 105]*. This process complicates the production of DSSCs and it's a one reason why solids hole-transfer materials (such as conductive polymers) are studied as an alternative to a liquid electrolyte.

10.5. Effects of Electrolyte Loss

The DSSCs constructed for this research are susceptible to a decrease in performance due to loss of the electrolyte. However, they can easily be "revived" by supplying new electrolyte. The plot of the recorded V_{OC} vs. time is shown in Figure 10-9. The V_{OC} of a DSSC increases after being left to dry for a week as electrolyte is slowly added by capillary action.

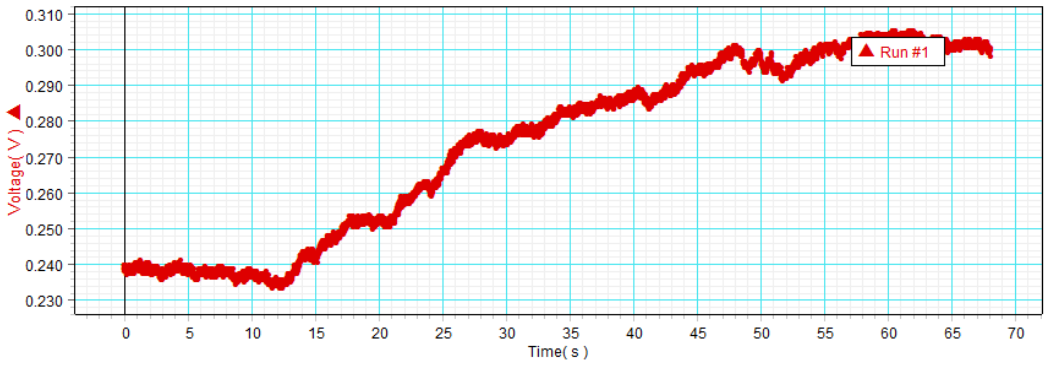

FIGURE 10-9: EFFECT OF ELECTROLYTE REPLENISHMENT ON VOLTAGE OUTPUT OF A DSSC

11.Ongoing Work

Work is currently being done to improve the efficiency of organic photovoltaics through the management of light trapping, up-conversion of infra-red (IR) light and improvements in the mobility of ions contained in the electrolyte. These improvements seek to engineer changes in the layer architecture of DSSC through easily available materials such as silica or TiO_2 nano-particles.

11.1. Scattering and Photon Up-conversion

The first technique being implemented is to improve the light trapping efficiency of DSSCs through the addition of a scattering layer. This technique is used to boost the light harvesting efficiency of photovoltaics that have active layers with a low coefficient of light absorption. Scattering layers improve the probability that a non-absorbed photon will be scattered back to a layer where it can be absorbed. The second technique under consideration evolved from previous research in thin-film photovoltaics by the Fortmann Group *[106]*. This technique will create a coated layer on the solar cell containing phosphorescent materials (phosphors). This layer will use Raman scattering (anti-Stokes) to up-convert IR photons to a wavelength more efficiently absorbed by the solar cell.

11.1.1. Light Management through Phosphors

Luminescence is any process where the light absorbed by a material is emitted at a different wavelength. It is possible to use the luminescence properties of phosphor to aid in the spectral management of solar light through the up-conversion of IR light. Phosphors are composed of a crystalline matrix of a “host material” within which impurities known as “activators” have been infused. The activator material is the one mostly responsible for the luminescence of light by the phosphor *[107, 108]*.

11.1.1.1. Theoretical considerations

Solar cells in general only capture a small range of the available solar spectrum (Figure 11-1). The range of capture is determined by the band-gap of the absorbing semiconductor as in the case of IPV's or the separation between the HOMO and LUMO energy states as in the case of DSSCs. The efficiency of solar cells at converting light into electrical power is very high at this narrow range. For instance, the single junction amorphous silicon solar cell with a semiconductor band gap of ~ 1.7 eV converts photons with wavelengths ranging from ~ 560 nm to ~650 nm with near 100% efficiency *[2]*.

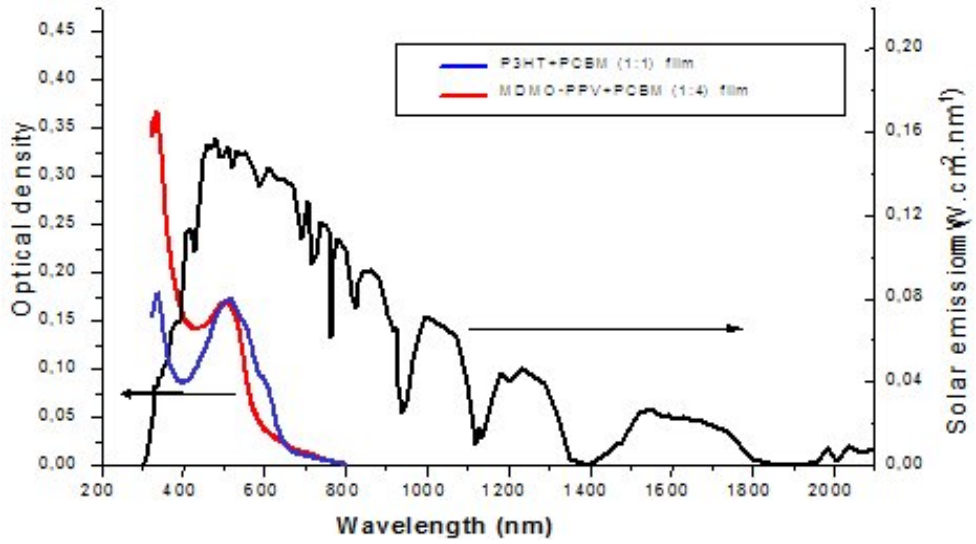

FIGURE 11-1. SOLAR SPECTRUM AND ABSORPTION SPECTRA OF HIGH PERFORMANCE ORGANIC SOLAR CELLS (HTTP://WWW-MOLYCELL.CEA.FR/ ; MOLYCELL)

Similarly, the photo-active layer in OPV's only capture light within a narrow range. As seen in Figure 11-1 some of the most high-performance OPV's are limited in the absorption to a relatively narrow range around 400 to 600 nanometers. To solve this problem it has been suggested to build tandem organic solar cells as it has been done previously with inorganic cells *[109]*. This will require the deposition of multiple layers of organic photo-active materials each sensitive to different bands of the solar spectrum *[27]*.

However, the addition of a tailored phosphor layer can be used to widen the spectral absorption range without the complexity of adding multiple layers of organic sensitizers. Up-converting phosphor coatings are a proven technology that has been available in the market for a long time. For instance, IR viewer cards used to visualize infra-red beams are common in research labs. The location of the coating on the cell is still to be decided. However, it will most probably be located at the back of the DSSC so it can up-convert and scavenge the near IR that could not be absorbed in its first past through the cell *[110]*.

11.1.1.2. Spectral up-conversion considerations

It is possible to use up-converting or "anti-Stokes" phosphors to shift light into regions of the solar spectrum more efficiently absorbed by the DSSC. The up-conversion process is mediated by the absorption of two photons sequentially ('two-step' or 'double photon'
process) *[111]*. The up-conversion layer to be added on the DSSCs will combine near-IR and visible-to-UV photons to emit a visible light photon in the range of ~500 nanometers. Therefore, this process will shift energy from the parts of the solar spectrum not efficiently absorbed by the dye or sensitizers to a region where is most efficient (~520 nanometers).

The phosphorescent layer to be added to the DSSC will consist of activator particles (element or compound to be decided) embedded in a matrix of the host material (TiO_2).

Light absorption through a solid can be described as *[12]*:

$$\Gamma_\lambda = \Gamma_{0\lambda} e^{-\alpha_\lambda L}$$

EQUATION 11-1: LIGHT ABSORPTION THROUGH A SOLID

In this equation Γ_λ is the remaining photon flux at wavelength λ after an initial photon flux of $\Gamma_{0\lambda}$ passes through a L thickness of semiconductor material that has an absorption coefficient α_λ at said wavelength λ. Therefore, an increase in semiconductor thickness L will result in more absorbed photons with a smaller remaining photon flux Γ_λ .

Scattering light to large angles is fundamental to the absorption/emission process since the emission processes are isotropic (emission is equivalent for all possible angles). Therefore, the phosphor layer should be capable to both up-convert photons and to scatter photons at large angles. This will lead to an increase in the path length of absorbable photons in the active layer of the DSSC.

The loss cone of a solar cell refers to range of light angles that upon incidence on the internal front surface are not trapped by total internal reflection but instead are reflected back into the air. As mentioned previously it is necessary to increase the path length of photons through a medium that is not an efficient absorber. This can be accomplished by the multiple passes through the photo-active medium resulting from total internal reflection. The smaller the loss cone angle, θ, the smaller the amount of lost light. The refractive index of the matrix controls the loss cone angle:

$$\sin\theta = \frac{n_1}{n_2}$$

EQUATION 11-2: TOTAL INTERNAL REFLECTION CONDITION

where n_1 is the refractive index of air (~1) and n_2 is the refractive index of the media. Clearly the larger the refractive index of the matrix the smaller the number of lost light photons as has been previously described by Winz et al. for the case of diffuse light scattering layers applied to the back of solar cells *[112]*.

Commercially available phosphors (e.g., Q42 from Lumitek® International, Inc.) emit through luminescence a visible light photon in ~ 600 nm range after absorption of IR and UV photons. Therefore, it can be possible to add a scattering and luminescence coating to the DSSC that will improve its overall light harvesting efficiency. This coating will be composed of Q42 within a high index media for example epoxy (n = 1.2) or a large band gap semiconductor (e.g., a-SiC:H:B with a band gap of 2.1 eV).

It is important for solar cell design flexibility that the light scattering and spectral changing layer should be highly conductive. When the up-conversion/scattering layer is conductive electric power can be harvested from the solar cell without the need and complexity of an underlying metal grid structure and/or conductive layer or material. The necessary conductivity can be realized by employing a doped semiconductor media such as p-aSiC:H:B material.

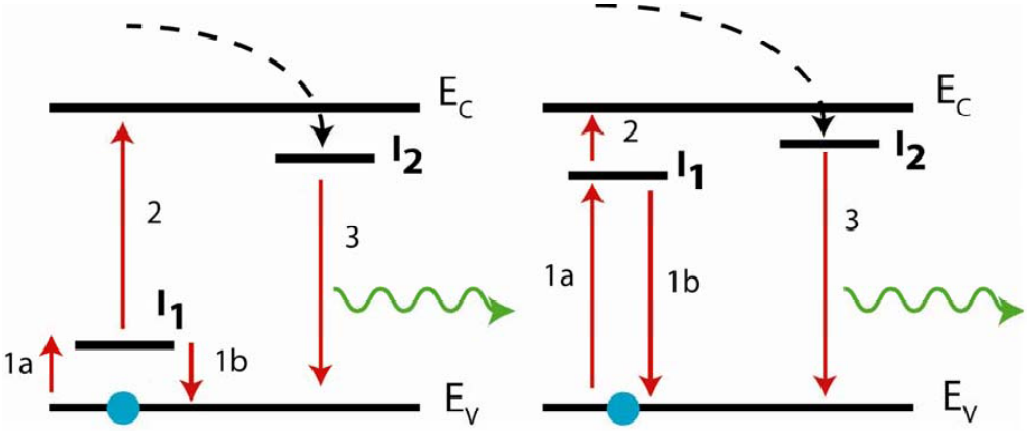

FIGURE 11-2: THE ENERGY LEVELS OF A SYSTEM THAT ABSORBS A UV PHOTON TO PROMOTE AN ELECTRON (BLUE CIRCLE) FROM LOWEST LEVEL, 1, TO INTERMEDIATE LEVEL 2, A THERMAL RELAXATION REDUCES THE ENERGY 3 AND A SUBSEQUENT TRANSITION 4 PRODUCES A VISIBLE LIGHT PHOTON. THE PHOTON FLUX Γ2 MUST BE SUFFICIENT TO OVERCOME A NON-RADIATIVE TRANSITION 1B BACK TO THE GROUND STATE.

An example of a system with electronic energy levels capable of providing up-conversion of two or more photons into one or more visible light photons is described with an idealized band diagram containing impurity levels illustrated in Figure 11-2. Preliminary modeling results indicate solar cell efficiency gains greater than 25% (e.g., bringing a 10% solar cell up to 12.5%).

This technology can easily be applied to organic as well as inorganic photovoltaics. For example thin-film amorphous silicon solar collects nearly all the photons between ~455 nm and ~725 nm. Therefore, an up converting phosphor placed on the front or back of a silicon solar cell would need to efficiently convert two near-IR photons between 725 nm and 780 nm to contribute a 10% gain in efficiency. An efficient UV/IR phosphor would need to convert photons between 385 nm and 455 nm and between 725 nm to 750 nm to contribute a 10% gain.

Gains greater than 10% are possible when utilizing a multi-photon near-IR up-conversion layer. There are approximately $7x10^{16}$ photons/s-cm^2 in the solar spectrum range between ~730 nm and ~940 nm wavelengths. Assuming the absorption of two near-IR photons per emitted visible photon would indicate theoretical conversion efficiency gains of 35%. Up-conversion of near-IR and IR is possible using such materials as the element Erbium and Yttrium doped silica-based ceramics *[113]*. Importantly, despite losing the energy contained in the UV part of the solar spectrum an all near-IR up-converter can be a useful for visible light scattering when embedded in a matrix of differing refractive index.

11.1.2. Light Management through Silica Particles

Research is being done to increase the trapping of light inside photovoltaics by adding a scattering layer of silica nano-particles. There are similar proposals to increase the trapping of light by adding spherical voids embedded in a matrix of nanocrystalline TiO_2 *[83, 114]*. The voids are created by adding micro-spheres of Styrofoam to the layer that is subsequently burned off during annealing leaving a void behind. Improvements in the light scattering of large angle rays using particles with a size greater than the matrix such as TiO_2 (anatase or rutile phases) or other materials such as ZrO_2 has also been studied *[83, 115]*.

The benefits of increased light trapping gained by a scattering layer must outweigh any losses by absorption of the scattering layer itself. Previous research at the Fortmann group *[106]* has demonstrated the possibility of using nano-particles not only to improved light scattering but that can also be used for spectral management (Figure 11-3).

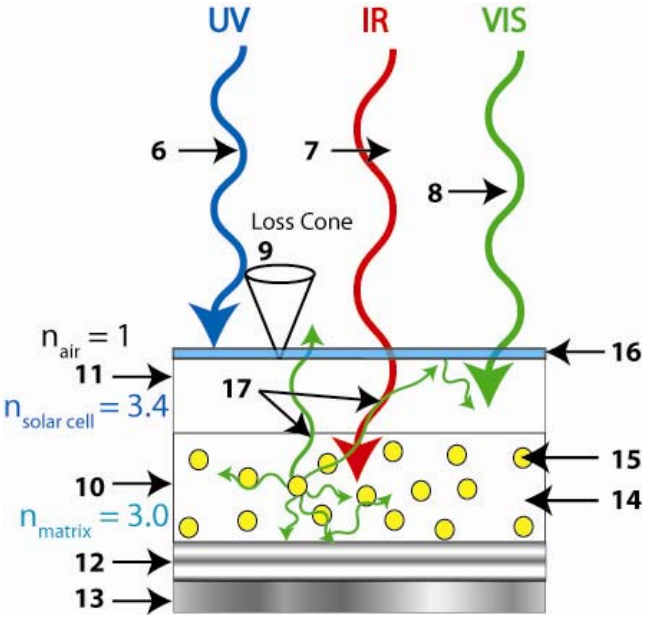

FIGURE 11-3. OPTICAL STACK FOR THIN FILM SEMICONDUCTORS INCORPORATING SCATTERING AND SPECTRUM CONVERSION LAYER.

Figure 11-3 shows the layer structure of scattering and solar spectrum modifying nano-particles embedded in a high refractive index matrix. The mechanics of light trapping are the same as mentioned before for the phosphor containing layer. The engineering problem is to control the loss cone as to maximize the amount of light trapped through internal reflection inside the solar cell (Equation 11-2).

Another application of silica nano-particles is the possibility of using the strong Raman anti-Stokes shift of silica to up-convert lower energy (IR) photons absorbed by the particles into more energetic ones (Figure 11-4). This process is based on the large Raman shift of silicon and has been demonstrated in practical applications such a silicon Raman shift based laser *[116]*.

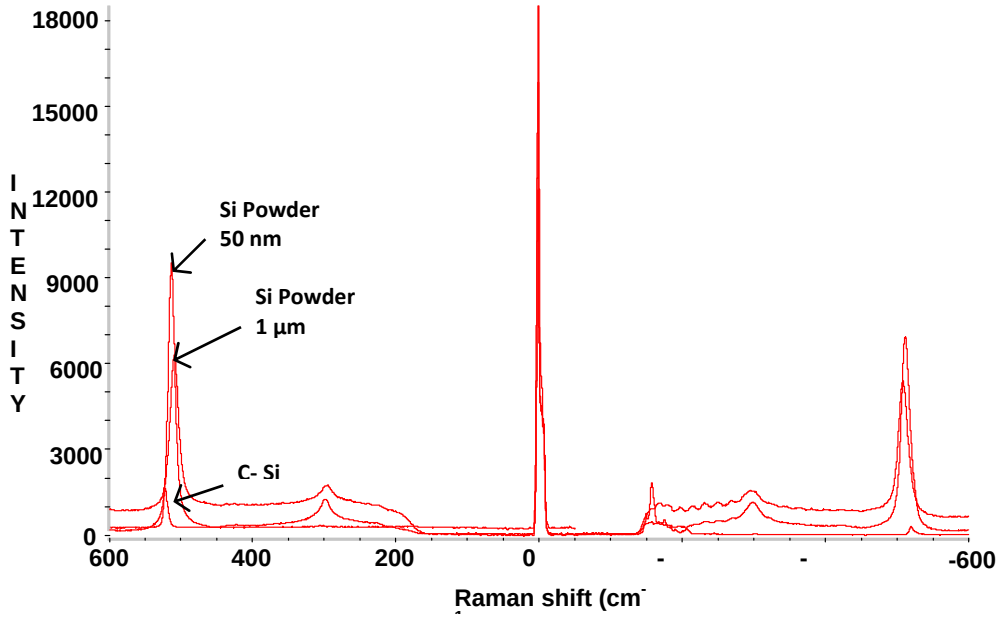

FIGURE 11-4. RAMAN STOKES AND ANTI-STOKES PEAKS OF SILICA POWDER OF DIFFERENT SIZES.

The intensity of the Raman shift it's possible to control by engineering the size of the silica nano-particles. The probability of decay for long wavelength phonons is very small inside nanometer sized particles. It has been shown that in amorphous (and nano-particle) silicon the phonon lifetime is exceptionally large *[106, 117]* when compared to single crystal silicon or other materials. Therefore the photon produced by one photon-phonon energy exchange is likely to be available for a second photon energy increasing phonon-photon energy change (anti-Stokes Raman shift). Silicon nano-particle-based Raman up and down conversion offers the possibility of not only increasing the trapping of light by scattering but also to transfer some of the energy lost in long wavelength photons to a spectral range better absorbed by the photo-active layer of DSSCs.

Silica powders available commercially of ~50 and~ 1000 nanometers were purchased and research has started on characterizing the Raman anti-Stokes shift strength for different particles sizes. The investigations on the particle size intensity dependence of the Raman shift with relation to the particle size are not constrained by the initial

particle size. Processes such as wet chemical (HF acid) etching techniques are being used to reduce the particle size.

A Thermo Nicolet Almega® micro-Raman spectrometer with a 785 nm probe beam has been used for the initial vibrational spectroscopy analysis of the silica powders. Initial studies in the anti-Stokes Raman shift of bulk silicon nano-particles shows a small shift to smaller wavenumbers (when compared to crystal silicon) and the expected large increase in amplitude. It is this increase in amplitude that is the foundation for the proposed spectral shift paradigm.

11.2. Hole diffusion gradient

The electrolyte contained within the DSSC must be able to rapidly shuttle charge carriers (holes and electrons) between the counter-electrode and the dye. However, current materials are limited in their rate of charge transfer by their relatively low diffusion constant that in the case of iodide and triiodide is in the range of $\sim 1\times 10^{-5} cm^2/s$ *[72]*. Therefore, solutions are needed that will inexpensively improve the diffusion and mobility of ions leading to an increase in the photovoltage and photocurrent produced by DSSCs.

11.2.1. Mobility Problem in Organic Photovoltaics (OPV)

One of the weaknesses in the current generation of liquid hole-transport layer (HTL - electrolyte) is the low mobility of ions (and/or electrons and holes in a solid polymer film case) through the layer. Despite their cost polymer HTL have remarkable low mobilities. For instance, oligothiophene,-based materials have mobilities less than $0.03 cm^2/V-s$, phthalocynines less than $0.01 cm^2/V-s$, pentacene less than $0.62 cm^2/V-s$, C^{60} less than $0.08 cm^2/V-s$, perylene-diimide $1.5\times 10^{-5} cm^2/V-s$ etc

[118]. The mobility of charges in aqueous solutions can be found from their diffusion constants using the Einstein relation:

$$mobility = \frac{D}{kT}$$

EQUATION 11-3: MOBILITY RELATIONSHIP

This relation indicates that for ions with diffusion constants in the $10^{-5}\,cm^2/s$ range the mobility is around $10^{-4}\,cm^2/V-s$ as demonstrated by Kang and Fortmann *[6]*. This low mobility affects the photovoltage since a portion of the potential must be used to aid in the driving of the ions thereby reducing the voltage available for external power generation.

The mobility values of OPV are very low compared to IPV. The values quoted for iodide and triiodide are small compared to the mobility of crystal silicon ($> 100 cm^2/V-s$) or amorphous silicon $\sim 1 cm^2/V-s$. It is possible to calculate the percentage of the photo voltage lost to drive ion or charge transport. For instance, the voltage V needed to provide an electric current, J_{sc}, of ~ 17 mA/cm^{-2} (parameters of common 10% efficiency solar cells) can be found form the expression:

$$J_{sc} \cong \mu N \frac{V}{d}$$

EQUATION 11-4: SOLAR CELL CURRENT AS A FUNCTION OF CARRIERS.

where: N = is the density of photo-generated carriers (assumed to be $10^{18} cm^{-2}$ for this illustration), d= the thickness of the region over which the charge must be transported (taken here to be around $0.5 \mu m$).

Using these values, and given a mobility of $5 \times 10^{-5} cm^{-2}/V-s$ and the previously stated value for the current, the needed voltage to drive the ions is 0.1 volts. This result implies that at least 20% of the voltage is not contributing to the final output (based on a V_{oc} of 0.5 volts).

11.2.2. Biologically Inspired Motive Force Gradient

Research done on neuronal ion transport by Kang and Fortmann (*[6]* Figure 11-5) has found that a motive force arises from the dielectric interactions between the protein lining of the neural channel and transporting ion. An analog of this motive force can be engineered in the HTL of DSSCs that could help ion conduction and reduce the voltage drain needed to transport charges.

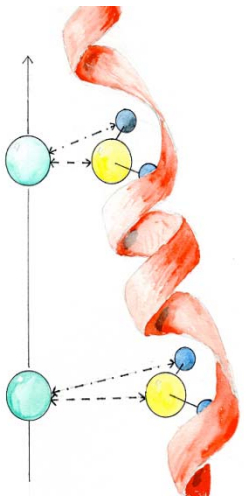

FIGURE 11-5: ION TRANSPORT IN NEURONS (KANG AND FORTMANN, 2007)

The mobility of a charge carrier under the influence of an electric field and a second energy field, $\nabla\Phi$, can be described as:

$$\mu = \frac{D\nabla \ln(n_p)}{\nabla\Phi + kT\nabla \ln n_p}$$

EQUATION 11-5: CHARGE MOBILITY UNDER AN ELECTRIC FIELD

where, n_p is the density of the ionized particles under consideration. The mobility is inversely proportional to the sum of the concentration gradient in the second energy field,

$\nabla\Phi$, and the product of kT and the gradient in concentration, n_p. As the sum in the denominator decreases there is an increase in the ion mobility that leads to an increase in the charge flow.

As mentioned previously (Equation 8-2) in DSSCs the photo-reaction consumes three iodine ions each with a single negative charge to produce a relatively dilute (low probability of interaction between clusters) three atom iodine-complex (triiodide) having a single negative charge. A positive charge of +2e (holes travelling towards the counter-electrode) is transported with each triiodide. As the ions in the electrolyte diffuse the triiodide interacts with its surrounding medium via polarization *[116]* and since the polarization reduces the ionic electric field energy (Figure 11-6), *W*, via:

$$W = -\frac{1}{2}\int_{V_1} (\varepsilon_1 - \varepsilon_0)\vec{E} \bullet \vec{E}_0 \, dx^3$$

EQUATION 11-6: ENERGY CHANGE DUE TO CHANGE OF POLARIZATION IN THE MEDIUM

where, ε_0 is the dielectric of free space, ε_1 is that of a media under consideration, and the vectorial quantities $\vec{E} = \frac{e}{\varepsilon_1 r^2}\hat{r}$ and $\vec{E}_0 = \frac{e}{\varepsilon_0 r^2}\hat{r}$.

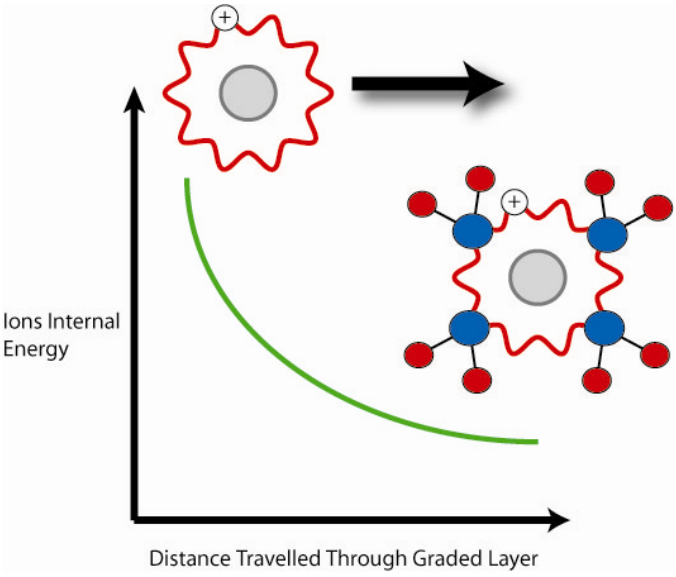

FIGURE 11-6: IONIC ENERGY REDUCTION GRADIENT BY ENVELOPMENT IN A HYDRATION SHELL (WATER MOLECULES)

Therefore, Equation 11-6 implies that an engineered gradient in the dielectric constant can be used to create an energy gradient (or force) defined by:

$$Force = \frac{\delta W}{\delta x} = \frac{\delta\left(-\frac{1}{2}\int_{V_1}(\varepsilon_1 - \varepsilon_0)\vec{E} \bullet \vec{E}_0 r^2 \sin\phi\, d\phi dr d\theta\right)}{\delta\varepsilon_1}\frac{\delta\varepsilon_1}{\delta x}$$

EQUATION 11-7: INDUCED ENERGY GRADIENT (FORCE) BY DIELECTRIC CHANGE IN THE MEDIUM

In the limiting case where $\varepsilon_0 >> \varepsilon_1$ and the only electric field acting on the travelling particle is the ionic field radiating outward from the ion under consideration Equation 11-7 can be written as:

$$Force = \frac{\delta W}{\delta x} \approx \frac{-1}{2}\int_{V_1} \frac{e^2}{\varepsilon^2_1 r^4} r^2 \sin\phi\, d\phi dr d\theta \frac{\delta\varepsilon_1}{\delta x} = \frac{2\pi(r^{-1} - a^{-1})}{\varepsilon_1^2}\frac{\delta\varepsilon_1}{\delta x}$$

EQUATION 11-8: LIMITING CASE OF INDUCED ENERGY GRADIENT

Where *a* is the minimum radius (that of the ion) and r can be taken to be separation half way to the next ion. From Equation 11-8 it is seen that a force results from a spatially dependent gradient in the dielectric constant, $\frac{\delta\varepsilon_1}{\delta x}$. Though application of Equation 11-8 with $\nabla\Phi \equiv \nabla W$ an enhancement in the ion mobility can be engineered. These calculations show that using readily available materials (e.g., TiO2, silica nano-particles) a gradient in the range of $600 eV/cm$ is possible by choosing water-based matrix with dielectric properties graded by nano-particles that have a closely matching ε_0 dielectric constant as shown in Figure 11-7.

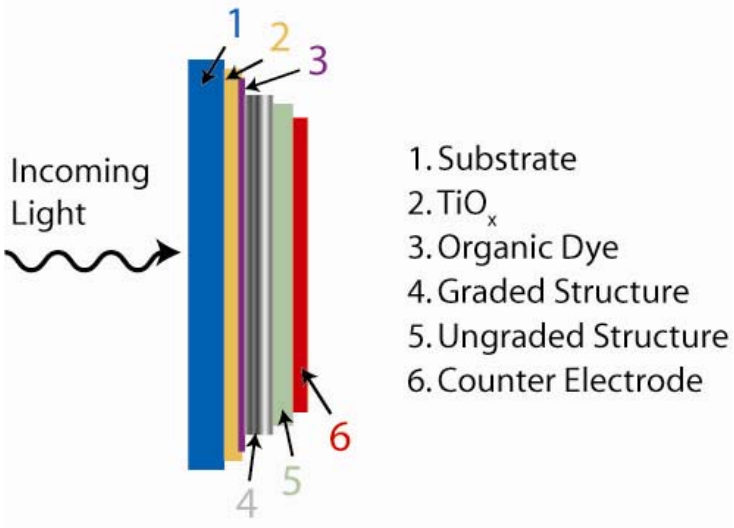

FIGURE 11-7. OPTICAL STACK FOR GRADED LAYER DSSC.

Initial testing on DSSCs using the structure shown in Figure 11-7 has been done and has shown an increase in the open circuit voltage V_{OC}. As shown in Table 5 there is an improvement in key photovoltaic parameters. Apart from the increased V_{OC} there is also an increase in R_{Shunt} that should decrease the photovoltage and photocurrent losses due to recombination. Also, there is an increase in the Fill Factor that increases the overall efficiency of the DSSC under external loads as compared to the standard DSSC. The non-optimized thickness of the applied layer had a detrimental effect on the R_{Series} factor. This increase in R_{Series} also leads to a reduction in the photocurrent JSC. Research is currently being done to find the optimal thickness of the graded spacing layer that will keep the improvement already noticed while also not affect or increasing J_{SC}.

Graded Layer	**V_{OC} (V)**	**J_{SC} (mA)**	**V_{Max} (V)**	**J_{Max} (mA)**	**R_{Shunt} (Ohms)**	**R_{Series} (Ohms)**	**Fill Factor**
Standard DSSC	0.477	1.08	0.290	0.77	1500	300→130	0.43
Cell with Alumina	0.493	0.541	0.352	0.402	4700	700→320	0.53

TABLE 5: : INITIAL TESTING ON THE EFFECTS OF SILICA NANO PARTICLES AS A GRADED AND GRADIENT LAYER

It should be mentioned that the enhancement in the transport of the oxidized electrolyte (triiodide) will be reduced by an inhibition of the iodide return flow. However, the motive force aiding the transport is inversely dependent on the concentration of the ions. In the DSSC studied for this research iodide has a concentration of 0.45 M and triiodide 0.05 M. Therefore, the transport of the iodide is not as affected. Analysis done has shown that losses in the photovoltage can be reduced by a properly engineered graded dielectric layer. Theoretically increases of up to 20% to the voltage can be achieved in DSSCs using nano-particles of alumina in a graded dielectric layer.

12.Future Perspectives on DSSC

Public and private funding in photovoltaics research and production has gone through high and low points. Previously the shock of the oil crisis in 1973 created a brief surge of government level support in alternative energy sources. The eventual decrease in the price of crude oil diminished some of the initiatives started during that period *[20]*. The rapid rise of crude oil prices usually restarts public and government interest in solar research as it happened during 2008 when the barrel of crude oil reached a price around $150. However, modern conditions are different compared to the 70's since crude oil price is not the only driving force in a search of non-hydrocarbon energy sources. The efforts to control and reduce causes of global warming will keep the public interest high that is needed to fund and implement a photovoltaics energy solution for the foreseeable future. The following are some of the main areas of interest for future investment in organic photovoltaics research. Also, the commercial aspects of DSSC manufacture and systems installation will be mentioned.

12.1. Research

Gains in efficiency and lowering of production cost are improving more rapidly with organic photovoltaics as compared to other technologies such as inorganic photovoltaics as seen in Figure 12-1. More improvements are expected as the DSSC and other organic photovoltaics technology continues to mature. These improvements may eventually lead to inexpensive organic photovoltaic modules. Some of the main avenues for robust improvement are better encapsulation techniques for ionic electrolytes and further research on natural organic dyes.

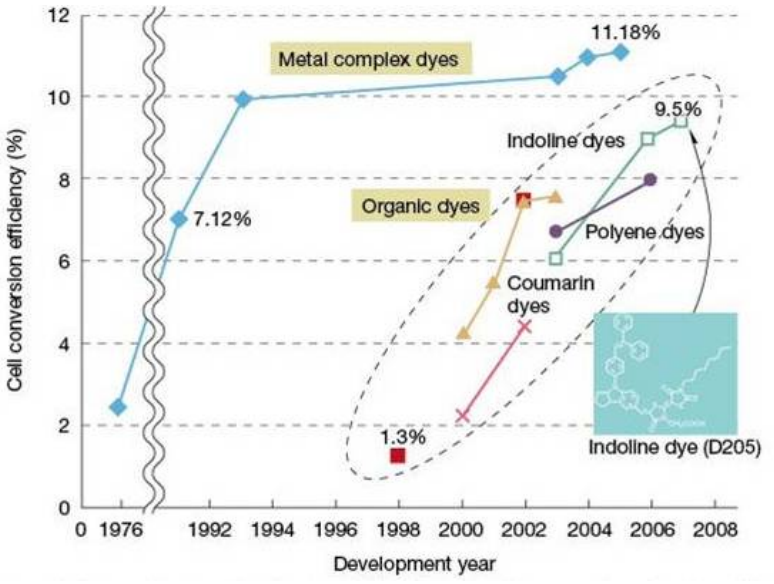

FIGURE 12-1: EFFICIENCY TRENDS FOR METAL COMPLEX AND ORGANIC DYES *[119]*

There are some drawbacks to using ionic liquid electrolytes (such as iodide/triiodide) despite the high performance and the research being done on different solutions to increase J_{SC} and V_{OC} (as found in this work) *[119]*. One of the drawbacks is that they tend to evaporate if not properly encapsulated and also a porous seal may permeate in water and oxygen and this may reduce the cell performance *[120]*. Also, when up-scaling solar modules it is necessary to add charge collection aids such as silver or aluminum bus bars. These materials are attacked by the liquid electrolytes currently being used such as the iodide/triiodide redox couple. As mentioned previously, there are materials available to encapsulate organic photovoltaics and keep the liquid electrolyte inside (glass-frit, Surlyn ^{tm} , *[103]*) . However, more research needs to be done on improved encapsulation techniques and materials.

An alternative to the problems inherent in liquid electrolyte encapsulation is to use solid hole conductors *[121-123]* to form polymer hole-transport materials (HTM) layers. However, these materials are handicapped by their low carrier mobility that limits cell efficiency and their cost. Research being done by the Fortmann group and presented in this thesis offers a solution to the mobility problem using graded spacer layers. These layers can be applied not only to liquid electrolytes but can also be applied to solid hole-

conducting layers. Further, research must be done on cheaper alternatives to the already develop polymer HTM as to widen their usage in organic photovoltaics.

One of the most commonly used sensitizers is compounds containing Ruthenium bipyridyl complexes *[58, 124, 125]*. However, these dyes contain transition heavy metals that are toxic and hard to synthesize and expensive *[126]*. As an alternative to Ruthenium dyes various sources of organic sensitizers have been proposed such as rose Bengal, fluorescein and rhodamine B, rosella and blue pea flowes *[58, 95, 127]*. These natural dyes do not have the high performance of Ruthenium dyes but their availability and relativity non-toxicity merits continued research on their usage with DSSCs.

Performance metrics for future dye research must be based on key performance parameters such as the need to absorb as much of the solar spectrum as possible. It must also be able to attach to the surface of the semi-conductor electrode (TiO_2, ZnO, SnO_2, WO_2, $BaTiO_3$). Future dyes must also have attachment groups needed such as carboxylate or phosphonate groups needed for anchoring to the surface of the oxide *[128]*. To maximize the generation of electric power it must have matching energy states with conduction band of oxide. A difference between the LUMO (dye) and conduction band (oxide) levels leads to losses in the photo-voltage. And finally to reach the desired goal of 20 year module lifetime the dye must be capable of sustaining 10^8 light absorption, injection and reduction cycles *[128]*.

12.2. Industrial Developments

The lower manufacturing cost of organic solar cells compared to their inorganic cousins and the rapid rate of efficiency improvements have caught the attention of the photovoltaics industry. Mass manufacturing techniques such as screen-printing, roll-to roll coating, drying and sintering can be used in the construction of OPV's*[83]*. A start-up by by Konarka (www.konarka.com) based in Lowell, MA, has opened a factory ready to produce organic solar cell in commercial quantities *[129]*. Other companies such as

G24 Innovations (www.g24i.com) and Peccel Technologies (www.peccell.com/en) have built or are in the process building plants to start the production of organic photovoltaics modules *[130]*. Figure 12-2 shows an example of the type of facilities were DSSC are to be produced.

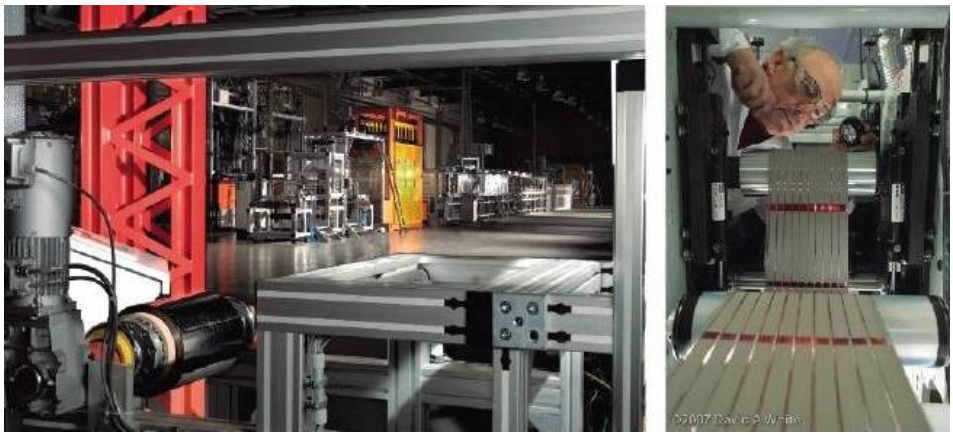

FIGURE 12-2: NEWLY DEVELOP ORGANIC SOLAR CELL MANUFACTURING PLANTS. ON THE LEFT THE G24I PLANT AND ON THE RIGHT A PLANT CONSTRUCTED BY KONARKA *[130].*

These developments clearly show that there is industrial interest in the production of organic photovoltaics. They also show that the U.S. Department of Energy (DOE) goals by 2020 to have organic photovoltaics systems with efficiency of 12% and cell degradation of less than 2% per 1000 hours are achievable *[131, 132]*. A study by the photovoltaics industry analyst firm NanoMarkets has forecast an increase in manufacturing capacity for thin-film and organic photovoltaics from 2 GWp (Gigawatts at peak sunlight) in 2008 to 29 GWp by 2015 *[133]*. There is obviously a lot of room for emerging organic and dye-sensitized photovoltaics technologies to compete and mature. The research presented in this thesis is one of the technologies that will help reach the goals stated by DOE.

12.3. Cost Analysis of Organic Photovoltaic

At the moment the cost of energy produced by the burning of hydrocarbon derivatives seems to be lower than the cost of energy produced by photovoltaic. However, this lower cost is an artifact produced by market forces that don't take into account accurately

tabulated hydrocarbon reserves. It also doesn't take into account the added environmental cost of exploration, extraction, transport, refining and consumption. It can be shown that the cost of implementation of organic solar cells can be comparable or cheaper than their inorganic cousins and a direct competitor to other types of energy generation. Energy payback time (EPBT) or time needed to generate the energy spent on manufacturing the system is an important metric that can be used to quantify whether a photovoltaic technology has economic potential. A report by the Energy research Center of the Netherlands (ECN) has shown that the payback time for DSSCs is around 1.4, 0.8 and 0.6 years for conditions in north-west Europe, south Europe and the Sahara respectively. These reported values as compared to the EPBT of 1.5 years for modules of multi-crystalline silicon shows the potential of organic photovoltaics as an alternative to inorganic cells *[134]*.

The cost of implementing a photovoltaics solution in the field can be separated into the cost of the modules and the cost of installation *[135]*. The components of these costs are the following:

Balance of modules (BOM)

- Materials cost, not only includes the cost of the materials contained in the module but also materials waste incurred during production. Improvements in manufacturing and process efficiency reduces this cost;
- Production cost, combines the cost of manufacturing such as equipment and energy usage during the process. It is obvious that the energy invested in manufacturing a solar cell must be lower than energy produced during the cell lifetime. The energy invested versus energy generated ratio (E_{inv}/E_{gen}) should always be minimized as this counts as a major part of the cost of the device;
- Overhead cost, comprises miscellaneous cost such as R&D expenses, technology licensing fees, advertisement, etc. The added cost related to the development of a particular technology tends to be high during the initial phase of production. However, this cost decreases substantially after the initial development cost has been recouped.

Balance of installation (BOS)

- Area and installation cost, this adds the cost incurred during installation of the module, renting of the occupied space (solar cell farms), mounting hardware, etc. The locations proposed for the construction of solar farms are located away from dense population centers and the purchase or renting cost per acre will tend to be low. The mounting hardware consist of off-the-shelf components with a relative low price;
- Energy transport cost, comprises the cost of power lines, voltage transformers and in general the infrastructure needed to transport and manage electricity. This cost adds up when the solar energy is collected far away from its intended utilization.

Organic photovoltaics will share the same installation cost compared with their inorganic counterparts. However, substantial reductions in the cost of the module can be achieved with organic photovoltaics. This is because the materials, production processes and infrastructure needed to support their manufacturing are not as energy intensive and do not use low availability or difficult to produce or synthesize materials. For instance, most of the materials needed in the production of OPV's can be mass produced by the chemical industry. In contrast, some IPV designs are dependent on the expensive and hard to scale up production of materials by the semiconductor industry (e.g., c-Si). Further reductions in cost can be expected as the technology of these organic devices continues to mature. These reductions will lead to a decrease in the EPBT of organic solar cells and their increase as part of the photovoltaic systems market share.

13. Concluding Remarks

This research has shown the potential of organic photovoltaic and in particular dye-sensitized solar cells to help fulfill the future needs of hydrocarbon free energy generation. The groundbreaking research initiated by Graetzel and others has opened the doors for a new type of photovoltaics that can compete with commercial inorganic solar cells in both cost of production and efficiency. Recent development on efficiency improvements can make organic photovoltaics a prime candidate for the renewable energy-based economy

Knowledge about the similarities and differences between inorganic and organic photovoltaics is a necessity. Some of the same idealizations such as the "equivalent circuit" model can be used to understand how the devices work. The field of organic photovoltaics owes its rapid advancement to the comprehensive body of research on inorganic solar cells. This groundwork has studied and solved many practical problems on how to model, construct, test and optimize devices that are applicable to both types of photovoltaics. Significant improvements on the efficiency of DSSC can be achieved despite the incomplete understanding on the factors that determine the photovoltage and photocurrent. As delineated in this dissertation, the relationships between relative positions of the energy levels of components of DSSCs are critical on the effective V_{OC} produced by the cells. Also, the application of the simple to understand "equivalent circuit" model has been used to identify recombination losses that affect V_{OC} and J_{SC}.

The components of the DSSC's analyzed in this research (e.g., TiO_2, conductive substrates, graphite, organic dye, etc...) are easy to acquire and assemble. Also, an affordable test-bench of photovoltaic properties has been constructed. This setup has been used to test changes on the construction parameters of DSSCs. Experimental I-V curves were fitted to the "equivalent circuit" model. Using this model idealized parameters such

as R_{Shunt}, R_{Series} and Fill Factor were used in conjunction with experimental values V_{OC}, J_{SC} and P_{Max} to characterize the photovoltaic properties of DSSC's.

The anthocyanin dye extracted from California blackberries (Rubus ursinus) was used as general purpose sensitizers in all the DSSC that were studied. Research on the quantum efficiency of DSSC and absorption spectroscopy of the dye was useful in finding in which part of the solar spectrum the cells were more efficient. The apparent shift on the wavelength dependent peak quantum efficiency and dye absorption has not been covered in detail within the available literature wavelenght ($\Delta \approx 27$ nanometers). However, it could be related to the lack or presence of a local aqueous environment as understood by previous work from Kang and Fortmann. The insights gathered during these experiments were helpful in gaining a deeper understanding on how DSSC work.

Research has been done on improvements to the performance of organic photovoltaics based on scattering layers to increase absorption of light and to the mobility of carriers using graded spacer layers. This research has shown the possibility of using easily available and affordable materials such as TiO_2 or silica nano-particles to increase the efficiency of organic and thin-film photovoltaics. Scattering and up-converting layers using Raman anti-Stokes shift can be used to more efficiently harvest the long-wavelength unused part of the solar spectrum (>550 nanometers). A way to improve the poor ionic mobility in solutions ($D \sim 10^{-5} cm^2/s$) has been shown using the drift field crated by a medium with a graded dielectric constant. Calculations have shown that theoretical increases of up 20% of the cell voltage can be achieved. The research done on ionic mobility aided by drift fields can be applied to liquid or solid hole conductive layers.

An overview has been given on future avenues for research in DSSC photovoltaics. Advancements in novel nature-inspired sensitizers can lead to lower production cost and better dye stability. Suitable dyes for tandem DSSC architecture could be found in nature. Improved encapsulation techniques could lead to continued use of liquid electrolytes (less expensive than solid electrolyte). The materials used to construct DSSC are far from

optimal and there are many research opportunities for new materials that can make DSSC cheaper, more efficient and not as susceptible to degradation.

Finally, many companies are starting production or are in the process of constructing manufacturing lines of DSSC and other types of organic solar cells. Calculated module costs for organic photovoltaics show an economical edge over their inorganic counterparts. The industrial interest on organic photovoltaics technology is high at the moment and this will lead to continued investment. There are still many areas for improvement such as photovoltaics module scalability, payback time and in particular the uncertainty on long-term degradation effects on the output of organic cells. However, there is a consensus that these problems will be solved as the technology matures or at least the problems will be mitigated.

14.References

[1] Ken Zweibel, National Renewable Energy Laboratory (NREL), **2005**.
[2] Carlson, *Semiconductors and Semimetals: Hydrogenated Amorphous Silicon, Part D*, Vol. 21, Academic, **1984**.
[3] Anders Hagfeldt and Michael Gratzel, *Accounts of Chemical Research* **2000**, *33*, 269.
[4] Brian O'Regan and Michael Gratzel, *Nature* **1991**, *353*, 737.
[5] Paul. Liska Nick. Vlachopoulos, Jan. Augustynski, Michael Graetzel, *Journal of the American Chemical Society* **1988**, *110*.
[6] Yeona Kang and C. M. Fortmann, *Applied Physics Letters* **2007**, *91*, 3.
[7] IEA PVPS Task 1, in *TRENDS IN PHOTOVOLTAIC APPLICATIONS*, IEA International Energy Agency, **2008**.
[8] The International Energy Agency (IEA), in *TRENDS IN PHOTOVOLTAIC APPLICATIONS*, **2008**.
[9] J.Paatero L.Oikkonen, T.Carlsson,P. Lund, Advanced Energy Systems - Helsinki University of Technology.
[10] Thomas Surek, *Journal of Crystal Growth* **2005**, *275*, 292.
[11] Richard H. Bube, *Photovoltaic Materials*, Imperial College Press.
[12] Bube Fahrenbruch, *Fundamentals of Solar Cells*, Academic, **1983**.
[13] Jenny Nelson, *Physics of Solar Cells*, Imperial College Press.
[14] Shinya Tsuda and Michitoshi Ohnishi Yukinori Kuwano, *Japanese Journal of Applied Physics* **1982**, *21*, 235.
[15] A. Cuevas and A. W. Blakers K. J. Weber, *Solar Energy Materials and Solar Cells* **1997**, *45*, 151.
[16] Harold J. Hovel, *Solar Cells*, Vol. II, Academic Press.
[17] Prof. Stephen Fonash - Penn State.
[18] Alexandre-Edmond Becquerel, *Comptes rendus de l'Académie des sciences* **1839**, *9*, 145 & 561.
[19] Charles Fritts, *Proceedings of the American Association for the Advancement of Science* **1883**, *33*.
[20] Antonio Luque and Steven Hegedus, *Handbook of Photovoltaic Science and Engineering*, Wiley, **2003**.
[21] Department of Energy (DOE).
[22] Armin G. Aberle, *Journal of Crystal Growth* **2006**, *287*.
[23] Ulrich Stutenbaeumer and Elias Lewetegn, *Renewable Energy* **2000**, *20*, 65.
[24] Maria Luisa Addonizio Lucia Vittoria Mercaldo, Marco Della Noce, Paola Delli Veneri, Alessandra Scognamiglio and Carlo Privato, *Applied Energy* **2008**.
[25] H. Schade A. V. Shah, M. Vanecek, J. Meier, E. Vallat-Sauvain, N.Wyrsch, U. Kroll, C. Droz and J. Bailat, *PROGRESS IN PHOTOVOLTAICS: RESEARCH AND APPLICATIONS* **2004**, *12*, 113.
[26] T. Söderström F.-J. Haug, M. Python, V. Terrazzoni-Daudrix, X. Niquille and C. Ballif, *Solar Energy Materials and Solar Cells* **2008**.
[27] B. de Boer A. Hadipour, P. W. M. Blom, *Advanced Functional Materials* **2008**, *18*, 160.

[28] Stuart Bowden Matthew Edwardsa, Ujjwal Das and Michael Burrows, *Solar Energy Materials and Solar Cells* **2008**, *92*, 1373.
[29] K.M. Hynes and I. Forbes R.W. Miles, *Progress in Crystal Growth and Characterization of Materials* **2005**, *51*, 1.
[30] N. Lakshminarayan Jaehyeong Lee, Suresh Kumar Dhungel, Kyunghae Kim and Junsin Yi, *Solar Energy Materials and Solar Cells* **2009**, *93*, 256.
[31] Jeffrey E. Cotter, *Journal of Applied Physics* **1998**, *84*.
[32] Kyunghae Kim Won Seok Choi, Junsin Yi and Byungyou Hong, *Materials Letters* **2008**, *62*, 577.
[33] E.V. Grushko and V.V. Motushchuk L.A. Kosyachenko, *Solar Energy Materials and Solar Cells* **2006**, *90*, 2201.
[34] A. Lakhtakia and S. Ashok, *Solar Energy Materials and Solar Cells* **1997**, *46*, 137.
[35] Paul D. Maycock, *Solar Energy Materials and Solar Cells* **1997**, *47*, 37.
[36] Pavel St'Ahel Petr Sladek, Pere Rocai Cabarrocas and Philippe Morin, *Philosophical Magazine B* **1998**, *77*, 1049.
[37] T. Brammer and H. Stiebig, *Journal of Applied Physics* **2003**, *94*.
[38] K.W. Kadam Jansen, S.B. Groelinger, J.F. , in *Conference Record of the 2006 IEEE 4th World Conference on Photovoltaic Energy Conversion*, **2006**.
[39] Howard M. Branz, *Solid State Communications* **1998**, *105*, 387.
[40] Brian A. Gregg and Mark C. Hanna, *Journal of Applied Physics* **2003**, *93*, 3605.
[41] Jun Ren Sheng Meng, and Efthimios Kaxiras, *Nano Letters* **2008**, *8*, 3266.
[42] Rachel Radspinner Sean E. Shaheen, Nasser Peyghambarian, *Applied Physics Letters* **2001**, *79*.
[43] Peter Chen Seigo Ito, Pascal Comte, Mohammad Khaja Nazeeruddin, Paul Liska, Peter Pechy and Michael Gratzel, *Progress in Photovoltiacs: Research and Applications* **2007**, *15*, 603.
[44] Marc Burgelman, "Thin Film Solar Cells by Screen Printing Technology", presented at *Microtechnology and Thermal Problems in Electronics*, Technical University of Lodz, **1998**.
[45] Toshiko MIZOKURO Xiaoliang MO, Hiroyuki MOCHIZUKI, Nobutaka TANIGAKI, and Takashi HIRAGA, *Japanese Journal of Applied Physics* **2005**, *44*, 656.
[46] Brian A. Gregg and Mark C. Hanna, *Journal of Applied Physics* **2002**, *93*, 3605.
[47] Tom Markvart and Luis Castañer, *Practical Handbook of Photovoltaics. Fundamental and Applications*, Elsevier, **2003**.
[48] Max Shtein & Stephen R. Forrest Fan Yang, *Nature Materials* **2005**, *4*, 37.
[49] V. Bulovi P. Peumans, and S. R. Forrest, *Applied Physics Letters* **2000**, *76*, 2650.
[50] Brian A. Gregg, *Chemical Physics Letters* **1996**, *258*, 376.
[51] Fan Yang and Stephen R. Forrest, *ACS Nano* **2008**, *2*, 1022.
[52] Christoph J. Brabec Sean E. Shaheen, and N. Serdar Sariciftci, *Applied Physics Letters* **2001**, *78*.
[53] Janke J. Dittmer Wendy U. Huynh, A. Paul Alivisatos, *Science* **2002**, *295*, 2425
[54] J. Gao G. Yu, J. C. Hummelen, F. Wudl, A. J. Heeger, *Science* **1995**, *270*, 1789
[55] Michael D. McGehee & Mark A. Topinka, *Nature Materials* **2006**, *5*, 675
[56] *Nanostructured materials for solar energy conversion*, Elsevier, **2006**.

[57] Michael Gratzel Andreas Kay, *Solar Energy Materials and Solar Cells* **1996**, *44*, 99.
[58] Kohjiro Hara and Hironori Arakawa, in *Handbook of Photovoltaic Science and Engineering*, (Ed: A. L. a. S. Hegedus), John Wiley & Sons, **2003**.
[59] Kohjiro Hara and Hironori Arakawa, in *Dye-sensitized Sola Cells*, (Ed: A. L. a. S. Hegedus), John Wiley & Sonds, **2003**.
[60] Michael Grätzel Greg P. Smestad, *Journal of Chemical Education* **1998**, *75*, 752.
[61] Z. Liu, *Journal of Molecular Structure: THEOCHEM* **2008**, *862*.
[62] Keld West Lasse Bay, Bjørn Winther-Jensen,Torben Jacobsen, *Solar Energy Materials and Solar Cells* **2006**, *90*, 341.
[63] Shogo Mori and Shozo Yanagida, in *Nanostructured Materials for Solar Energy Conversion*, (Ed: T. Soga), Elsevier, **2006**, 193.
[64] François Pichot and Brian A. Gregg, *Journal of Physical Chemistry B* **2000**, *104*, 6.
[65] Simona Fantacci Filippo De Angelis, Annabella Selloni, Michael Grtzel, and Mohammed K. Nazeeruddin, *Nano Letters* **2007**, *7*, 3189.
[66] Shigenori Tanaka and Shuzi Hayase Toshihiro Oda, *Solar Energy Materials and Solar Cells* **2006**, *90*, 2696.
[67] Greg P. Smestad Nerine J. Cherepy, Michael Gratzel, and Jin Z. Zhang, *Journal of Physical Chemistry B* **1997**, *101*, 9342.
[68] Shanqing Zhang Hua Yu, Huijun Zhao, Geoffrey Will, Porun Liu, *Electrochimica Acta* **2008**.
[69] and L. M. Peter P. J. Cameron, *The Journal of Physical Chemistry B* **2005**, *109*.
[70] Tatsuo Mori Masaki Murayama, *Thin Solid Films* **2006**, *509*, 123.
[71] M. Willander Suresh C. Jain, Vikram Kumar, *Conducting Organic Materials and Devices*, AP.
[72] Rolf Stanglb and Joachim Luther Jörg Ferbera, *Solar Energy Materials and Solar Cells* **1998**, *53*, 29.
[73] Yasuo Kimura Ken-ichi Ishibashi, and Michio Niwano, *Journal of Applied Physics* **2008**, *103*.
[74] Ashraful Islam Naoki Koidea, Yasuo Chibaa and Liyuan Han, *Journal of Photochemistry and Photobiology A: Chemistry* **2006**, *182*, 296.
[75] S. Bowden and A. Rohatgi, School of Electrical and Computer Engineering - Georgia Institute of Technology.
[76] D. Psych A. Mette, G. Emanuel, D. Erath, R. Preu and S. W. Glunz, *Progress in Photovoltiacs: Research and Applications* **2007**, *15*, 493.
[77] V. N. Singh and R. P. Singh, *Journal of Physics D: Applied Physics* **1983**, *16*, 1823.
[78] Georgina Ponce Alfredo Olea, P.J. Sebastian, *Solar Energy Materials and Solar Cells* **1999**, *59*, 137.
[79] Michael Gratzel, *Philosophical Transactions from the Royal Society A* **2007**, *365*, 993.
[80] Michael K.H. Leung and Dennis Y.C. Leung Meng Ni, *The Canadian Journal of Chemical Engineering* **2008**, *86*.
[81] L. Bay and K. West, *Solar Energy Materials and Solar Cells* **2005**, *87*, 613.

[82] Roberto Gómeza and Pedro Salvadorb, *Solar Energy Materials and Solar Cells* **2005**, *88*, 377.
[83] N.J. Bakker J.M. Kroon, H.J.P. Smit, P. Liska, K.R. Thampi, P. Wang, S.M. Zakeerudin, M. Gratzel, A. Hinsch, S. Hore, U. Wurfel, R. Sastrawan, J.R. Durrant, E. Palomares, H. Pettersson, T. Gruszecki, J. Walter, K. Skupien and G.E. Tulloch, *Progress in Photovoltiacs: Research and Applications* **2006**.
[84] Xizhe Liu Zhen Huang, Kexin Li, Dongmei Li, Yanhong Luo, Hong Li,Wenbo Song, LiQuan Chen, Qingbo Meng, *Electrochemistry Communications* **2007**, *9*, 596.
[85] Seigo Ito Takurou N. Murakami, Qing Wang, Md. Khaja Nazeeruddin, Takeru Bessho, Ilkay Cesar, Paul Liska, Robin Humphry-Baker, Pascal Comte, Péter Péchy, and Michael Grätzel, *Journal of The Electrochemical Society* **2006**, *153*, A2255.
[86] Jacques E. Moser Yasuhiro Tachibana, Michael Grätzel, David R. Klug, and James R. Durrant, *The Journal of Physical Chemistry* **1996**, *100*, 20056.
[87] John B. Asbury Randy J. Ellingson, Sue Ferrere, Hirendra N. Ghosh, Julian R. Sprague, Tianquan Lian, and Arthur J. Nozik, *The Journal of Physical Chemistry B* **1998**, *102*, 6455.
[88] Jihuai Wu Sancun Hao, Yunfang Huang and Jianming Lin, *Solar Energy* **2006**, *80*, 209.
[89] U. Opara Krašovec M. Berginc, M. Hočevar, M. Topič, *Thin Solid Films* **2008**, *516*, 7155.
[90] Zhengxi Zhang Li Yang, Shaohua Fang, Xuhui Gao, Masamichi Ota, *Solar Energy* **2007**, *81*, 717.
[91] Thanks for Katarzyna M. Sawicka for her help with the electro-spinning setup.
[92] Jaakko Saarinen and Peter Lund Janne Halme, *Solar Energy Materials and Solar Cells* **2006**, *90*, 887.
[93] David B. Lenhert Samuel L. Manzello, Ahmet Yozgatligil, Michael T. Donovan, George W. Mulholland, Michael R. Zachariah, Wing Tsang, *Proceedings of the Combustion Institute* **2007**, *31*, 675.
[94] Neyde Yukie Murakami Iha Andre Sarto Polo, *Solar Energy Materials and Solar Cells* **2006**, *90*, 1936.
[95] Vissanu Meeyoo Khawanchit Wongcharee, Sumaeth Chavadej, *Solar Energy Materials and Solar Cells* **2007**, *91*, 566.
[96] Bernard O. Aduda and Julius M. Mwabora Justus Simiyu, in *From Colloids to Nanotechnology: 8 Conference on Colloid Chemistry, Keszthely, Hungria, Septiembre, 2002.*, Springer, **2002**, 34.
[97] Hengyao Hu Dongshe Zhang, Laifeng Li and Donglu Shi, *Journal of Nanomaterials* **2008**.
[98] Thanks to Aruna Devi for her help assembling and making the monochromator operational.
[99] National Renewable Energy Laboratory (NREL).
[100] Yuki Uchida Takeshi Yamaguchi, Shinya Agatsuma and Hironori Arakawa, *Solar Energy Materials and Solar Cells* **2009**.
[101] Dr. H. Egeter Prof. Ernst Bayer, A. Fink, K. Nether, K. Wegmann, *Angewandte Chemie International Edition in English* **2003**, *5*, 791
[102] Personal discussion with Charles Fortmann - Discussion on anthocyanin molecule and the influence of enviroment on absorption and quantum efficiency of DSSC., **2009**.

[103] J. Beier R. Sastrawana, U. Belledin, S. Hemming, A. Hinsch, R. Kern, C. Vetter, F.M. Petrat, A. Prodi-Schwab, P. Lechne and W. Hoffmann, *Solar Energy Materials and Solar Cells* **2006**, *90*, 1680.
[104] Hanke K. P., *Zeitschrift für physikalische Chemie* **1999**, *212*, 1.
[105] J. M. Kroon A. Hinsch, R. Kern, I. Uhlendorf, J. Holzbock, A. Meyer, J. Ferber *Progress in Photovoltiacs: Research and Applications* **2001**, *9*, 425
[106] S. G. Chawda J. A. Mawyin, C. R. Clayton, R.J. Tonucci, C. M. Fortmann, "Substrate Engineering for High Efficiency Solar Cells", presented at *Materials Research Society - Spring Meeting*, San Francisco, **2008**.
[107] William M. Yen and Marvin J. Weber, *Inorganic Phosphors: Compositions, Preparations and Optical Properties*, CRC.
[108] Shionoya and Yamamoto Yen, *Fundamentals of Phosphors*, CRC, **2006**.
[109] S. Siebentritt S. Nishiwaki, P. Walk, M. Ch. Lux-Steiner, *Progress in Photovoltaics: Research and Applications* **2003**, *11*, 243
[110] B.S. Richardsc and M.A. Greena A. Shalava, *Solar Energy Materials and Solar Cells* **2007**, *91*, 829.
[111] Xiyan Zhanga Liping Lu, Zhaohui Baia and Xiaoyun Mi, *Materials Research Bulletin* **2009**, *44*, 207.
[112] C. M. Fortmann K. Winz, Th. Eickhoff, C. Beneking, H. Wagner, H. Fujiwara, I. Shimizu, *Solar Energy Materials and Solar Cells* **1997**, *49*, 195.
[113] George R. Fern Anne Newport, Terry Ireland, Robert Withnall, Jack Silver and Aron Vecht, *Journal of Materials Chemistry* **2001**, *11*, 1447
[114] Peter Nitz Sarmimala Hore, Carmen Vetter, Christof Prahl, Michael Niggemann and Rainer Kern, *Chemical Communications* **2005**, 2011.
[115] Carmen Vetterb Sarmimala Horea, Rainer Kerna, Herman Smitc and Andreas Hinsch, *Solar Energy Materials and Solar Cells* **2006**, *90*, 1176.
[116] Richard Jones Haisheng Rong, Ansheng Liu, Oded Cohen, Dani Hak, Alexander Fang and Mario Paniccia, *Nature* **2005**, *433*, 725.
[117] John David Jackson, *Classical Electrodynamics 3rd edition*, Wiley, **1999**.
[118] Gilles Horowitz, *Advanced Materials* **1998**, *10*.
[119] T. Horiguchi K. Hara, T. Kinoshitab, K. Sayama, H. Arakawa, *Solar Energy Materials and Solar Cells* **2001**, *70*, 151.
[120] Liduo Wang Bin Li, Bonan Kang, Peng Wang, Yong Qiu, *Solar Energy Materials and Solar Cells* **2006**, *90*, 549.
[121] Winfried Schaffrath Jtirgen Hagen, Peter Otschik, Ralf Fink, Andreas Bacher, Hans-Werner Schmidt, Dietrich Haarer, *Synthetic Materials* **1997**, *89*, 215.
[122] C.J. Brabec D. Gebeyehu, N.S. Sariciftci, *Thin Solid Films* **2002**, *403-404*, 271.
[123] G.R.R.A. Kumara K. Tennakone, I.R.M. Kottegoda, V.P.S. Perera, P.S.R.S. Weerasundara, *Journal of Photochemistry and Photobiology A: Chemistry* **1998**, *117*, 137.
[124] Thierry Renouard Peter Pchy, Shaik M. Zakeeruddin, Robin Humphry-Baker,, Paul Liska Pascal Comte, Le Cevey, Emiliana Costa, Valery Shklover,, Glen B. Deacon Leone Spiccia, Carlo A. Bignozzi, and Michael Grtzel, *Journal of American Chemical Society* **2001**, *123*, 1613.
[125] R.-A. Fallahpour T. Renouard, Md. K. Nazeeruddin, R., S. I. Gorelsky Humphry-Baker, A. B. P. Lever, and M. Grtzel, *Inorganic Chemistry* **2002**, *41*, 367.

[126] Tasuku Komori Yutaka Amao, *Biosensors and Bioelectronics* **2004**, *19*, 843.
[127] André Sarto Polo and Neyde Yukie Murakami Iha, *Solar Energy Materials and Solar Cells* **2006**, *90*, 1936.
[128] Michael Gratzel, *Journal of Photochemistry and Photobiology A: Chemistry* **2004**, *164*, 3.
[129] Kevin Bullis, in *Technology Review*, **2008**.
[130] Tetsuo Nozawa, in *Nikkei Electronics Asia*, **2008**.
[131] Dave Ginley, (Ed: U. S. D. o. Energy).
[132] Rick Matson, (Ed: U. S. D. o. Energy), **2007**.
[133] NanoMarkets, **2008**.
[134] A.C. Veltkamp M.J. de Wild-Scholten, in *Solar Energy*, Energy research Center of the Netherlands (ECN) **2007**.
[135] Vladimir Dyakonov Cristoph Brabec, Ullrich Scherf, *Organic Photovoltiacs: Materials, Device Physics and Manufacturing Technologies*, Wiley-VCH.